

# Simulation-based inference for stochastic nonlinear mixed-effects models with applications in systems biology

Henrik Häggström<sup>1</sup>, Sebastian Persson<sup>1</sup>, Marija Cvijovic<sup>1</sup>, Umberto Picchini<sup>1\*</sup>

<sup>1</sup>Department of Mathematical Sciences, Chalmers University of Technology and the University of Gothenburg, Gothenburg, Sweden.

\*Corresponding author(s). E-mail(s): [picchini@chalmers.se](mailto:picchini@chalmers.se);  
Contributing authors: [henhagg@chalmers.se](mailto:henhagg@chalmers.se); [sebastian.persson@crick.ac.uk](mailto:sebastian.persson@crick.ac.uk);  
[marija.cvijovic@chalmers.se](mailto:marija.cvijovic@chalmers.se);

## Abstract

The analysis of data from multiple experiments, such as observations of several individuals, is commonly approached using mixed-effects models, which account for variation between individuals through hierarchical representations. This makes mixed-effects models widely applied in fields such as biology, pharmacokinetics, and sociology. In this work, we propose a novel methodology for scalable Bayesian inference in hierarchical mixed-effects models. Our framework first constructs amortized approximations of the likelihood and the posterior distribution, which are then rapidly refined for each individual dataset, to ultimately approximate the parameters posterior across many individuals. The framework is easily trainable, as it uses mixtures of experts but without neural networks, leading to parsimonious yet expressive surrogate models of the likelihood and the posterior. We demonstrate the effectiveness of our methodology using challenging stochastic models, such as mixed-effects stochastic differential equations emerging in systems biology-driven problems. However, the approach is broadly applicable and can accommodate both stochastic and deterministic models. We show that our approach can seamlessly handle inference for many parameters. Additionally, we applied our method to a real-data case study of mRNA transfection. When compared to exact pseudomarginal Bayesian inference, our approach proved to be both fast and competitive in terms of statistical accuracy.

**Keywords:** hierarchical models, likelihood-free inference, stochastic differential equations, stochastic chemical reactions

## 1 Introduction

The analysis of data arising from multiple experiments — such as observations of individuals across various domains (e.g., humans, animals, cells, or trees) — has traditionally been approached using mixed-effects models ([Diggle et al. 2002](#); [Lavielle 2014](#)). These models account for individual variability by treating model parameters as random variables that vary between subjects, allowing a

hierarchical representation of the data. This structure effectively disentangles different sources of variability, distinguishing intra-individual fluctuations from between-individual differences. Mixed-effects modeling is widely applied across diverse fields, including biology, pharmacokinetics and pharmacodynamics, forestry, sociology, and many other disciplines where understanding variability across individuals is essential ([Davidian and Giltinan 2003](#)). The literature to tackle the inference

problem for mixed-effects models is vast. However, options reduce substantially when stochastic dynamical models are considered due to considerably increased theoretical and computational difficulties. In this work, we present a new strategy for Bayesian inference in hierarchical non-linear stochastic models with mixed-effects. Our approach provides fast to train *semi-amortized* approximations to both the likelihood function and the posterior distribution. We show that this makes our methodology scalable for an increasing number of individuals. In particular, we consider stochastic models with time-dynamics, with a focus on stochastic differential equations (SDEs) with mixed-effects. However, this is merely to provide illustrative case studies, as the methodology we introduce is agnostic to the specific type of model used to describe data.

Inference for stochastic modelling with mixed-effects is a challenging area due to the difficulty in (numerically) integrating out the latent quantities that enter the likelihood function. For example, models for stochastic chemical reactions that are common in systems biology involve either exact simulators (e.g. the Stochastic Simulation Algorithm, Gillespie 1977, the Extrande method, Voliotis et al. 2016) or approximate simulators (Gillespie 2000, Gillespie 2007), and all these make the likelihood function *intractable*, that is, it is not possible to evaluate it exactly and is computationally hard to approximate. For example, when the model is an SDE, and observations are available at discrete time points, the likelihood function is typically intractable (except for the simplest toy models) due to the unavailability of closed-form transition densities. The statistical literature to tackle such difficulty is vast, see eg. Craigmile et al. (2023) for a recent review. On top of such difficulty, when SDEs are embedded in a mixed-effects framework, the problem becomes even harder due to the increased dimension of the integration problem. Although the literature for mixed-effect SDEs is available, as collected in Picchini (2024), this is very specialized, as methods either tackle very specific models, lacking generality and well-maintained software, or are general but computationally very intensive, e.g. when based on particle-filters (Botha et al. 2021; Wqvist et al. 2021; Persson et al. 2022).

In this work, we provide a general approach for Bayesian inference in mixed-effects models

having intractable likelihoods, using simulation-based inference (SBI) (see Cranmer et al. 2020 for a review). The appeal of SBI methods is that these only require forward-simulation of the model, rather than the evaluation of a potentially complicated expression for the likelihood function, assuming it is available. This allows for approximate frequentist and Bayesian inference, whenever running the model simulator at many values of a parameter  $\theta$  is computationally not too onerous. Indeed, in SBI, simulated data  $\mathbf{y}$  are generated as  $\theta \rightarrow \mathcal{M}(\theta) \rightarrow \mathbf{y}$ , where the *simulator*  $\mathcal{M}$  can be any generative model. Provided with many pairs of simulated  $\theta$ 's and  $\mathbf{y}$ 's, it is possible to build inference for given observed data  $\mathbf{y}_o$ , in absence of a readily available expression for the likelihood function  $p(\mathbf{y}_o|\theta)$ , as we briefly summarize in Section 2. In recent years many SBI methods have focused on using deep neural networks to approximate conditional densities (“neural conditional density estimation”), for example to provide approximations to the posterior  $p(\theta|\mathbf{y}_o)$ , the likelihood  $p(\mathbf{y}_o|\theta)$ , or both, see Section 2 for key references. In our work, we obtain scalable and accurate inference for complex stochastic models with mixed-effects, without using neural conditional density estimation. We build on the *SEquential Mixtures Posterior and Likelihood Estimation* (SeMPLE) methodology (Häggström et al. 2024), which efficiently fits training data using a Gaussian mixture model via an expectation-maximization algorithm. The fitted Gaussian mixture provides, simultaneously, a closed-form deterministic approximation to both the likelihood and the posterior, which can both be evaluated and sampled from in a Gibbs sampler. For the case where  $M$  individuals are considered, with corresponding observed data  $\mathbf{y}_o^{(i)}$  ( $i = 1, \dots, M$ ), the surrogates of the likelihood and the posterior constructed by SeMPLE are called “semi-amortized”, since an initial amortized approximation of the likelihood  $p(\mathbf{y}|\theta)$  for a generic  $\mathbf{y}$  is first obtained, and then rapidly adapted to the individual-specific data  $\mathbf{y}_o^{(i)}$ , providing an approximation to the individual  $p(\mathbf{y}_o^{(i)}|\theta)$ , without having to re-start separate fittings completely from scratch for every individual  $i$ , but instead starting from the amortized approximation.

We present two versions of SeMPLE, both delivering accurate inference, as demonstrated

through comparisons with exact (pseudomarginal) Bayesian inference. The first version offers greater flexibility by allowing the specification of both fixed parameters and random effects, although at a higher computational cost. In contrast, the second version is designed for enhanced scalability, but requires all parameters to be treated as random effects. To illustrate our methodology, we applied it to three case studies: a mixed-effects Ornstein-Uhlenbeck state-space model and a mixed-effects SDE model used to describe translation kinetics following mRNA transfection. The latter model is examined using both simulated and real-world data. The code is available at [https://github.com/henhagg/semple\\_mem](https://github.com/henhagg/semple_mem).

## 2 Related work

Simulation-based inference (SBI) methods, reviewed e.g. in [Cranmer et al. \(2020\)](#) and [Pesonen et al. \(2023\)](#), have also been called “likelihood-free inference”, where the latter has been used especially with reference to approximate Bayesian computation (ABC) ([Marin et al. 2012](#); [Sisson et al. 2018](#)), synthetic likelihoods ([Wood 2010](#); [Price et al. 2018](#)) and, partially, pseudomarginal Markov chain Monte Carlo methods ([Andrieu and Roberts 2009](#); [Andrieu et al. 2010](#)) when simple forward simulation is possible (as when the bootstrap filter is used to unbiasedly approximate the likelihood). The mentioned approaches have also been denoted as “statistical SBI” in [Wang et al. \(2024\)](#), to distinguish those from more recent methods exploiting neural networks (typically normalizing flows, [Rezende and Mohamed 2015](#); [Papamakarios et al. 2021](#)) to approximate conditional densities, so-called neural conditional density estimation (NCDE), which have gained considerable attention. NCDE has been used to approximate likelihoods ([Papamakarios et al. 2019](#); [Chen et al. 2021](#)), posterior distributions ([Papamakarios and Murray 2016](#); [Greenberg et al. 2019](#); [Durkan et al. 2020](#); [Chen et al. 2021](#); [Miller et al. 2021](#); [Delaunoy et al. 2022](#)), or the likelihood and the posterior simultaneously ([Wiqvist et al. 2021](#); [Radev et al. 2023](#)). Moreover, NCDE approaches have been used both to sequentially refine inference conditionally on a specific observed data set  $\mathbf{y}_o$ , but also in an amortized way, see the review in [Zammit-Mangion et al. \(2024\)](#). For amortized

approaches, the trained network does not depend on any specific  $\mathbf{y}_o$  and therefore, once training has completed, it can be used to rapidly produce conditional density estimation for any  $\mathbf{y}_o$ , though this happens at a large upfront resource investment to obtain the amortized network in the first place. Regarding non-amortized approaches, comparisons between some of the methods are available, e.g., in [Greenberg et al. \(2019\)](#) and [Häggström et al. \(2024\)](#).

For the specific case of non-SBI inference for mixed-effects stochastic dynamic models, the range of inference options is large ([Picchini 2024](#)). However, this range shrinks considerably when SBI methods are considered: for the latter, methods for mixed-effects stochastic dynamic models revolve almost exclusively around pseudomarginal MCMC (pMCMC) ([Whitaker et al. 2017](#); [Wiqvist et al. 2021](#); [Botha et al. 2021](#); [Persson et al. 2022](#)), and an exception within SBI is the NCDE-based posterior inference in [Arruda et al. \(2024\)](#). The advantage of pMCMC methods is that they produce exact Bayesian inference in the limit of an infinite number of MCMC iterations. Therefore, when it is possible to use pMCMC, this provides gold-standard Bayesian inference. However, in practice, for pMCMC to be effective, advanced proposal mechanisms for the solution paths of the models are often needed, to reduce the variance of Monte-Carlo based likelihood approximations (typically via particle filters) and hence reduce the runtime to properly explore the posterior surface. In pMCMC, constructing proposals for the solution’s paths is a challenging and highly-specialized task (examples are [Golightly and Wilkinson 2011](#); [Del Moral and Murray 2015](#); [Schauer et al. 2017](#)), and bespoke constructions often need to be produced for any different attempted model and often depend on specific assumptions on the measurement error (e.g. a linear observation model with Gaussian measurement error). Moreover, the tuning of the parameter proposal in pMCMC (and especially its initialization) can be tedious and prone to trial-and-error. This is why alternative SBI methods that rely solely on “simple” *forward* model simulation are particularly appealing, as they facilitate learning the mapping between simulated  $\boldsymbol{\theta}$  and simulated  $\mathbf{y}$ . In our work, the goal is to construct surrogate deterministic approximations of the likelihood and posterior, rather

than stochastic likelihood approximations as generated in pMCMC. In doing so, we do not employ neural conditional density estimation, in contrast to [Arruda et al. \(2024\)](#), and instead provide a more parsimonious framework which is nevertheless expressive enough to produce accurate Bayesian inference. Before moving further, we wish to remind the reader that in SBI it is typical to conduct inference based on a “summarization”  $S(\mathbf{y})$  (provided by a data-reduction mapping) of  $\mathbf{y}$ , rather than inference based on  $\mathbf{y}$  itself, where  $S(\mathbf{y})$  is a set of statistics of  $\mathbf{y}$  that are deemed informative about  $\boldsymbol{\theta}$  ([Fearnhead and Prangle 2012](#); [Wiqvist et al. 2019](#); [Åkesson et al. 2021](#)) but are low-dimensional compared to  $\mathbf{y}$ . In our examples we do not consider data-summarization, and therefore we do not discuss this aspect further, however our methodology could accommodate inference based on some  $S(\mathbf{y})$  should it be necessary, and in such case all the instances where  $\mathbf{y}$  appears could be substituted with  $S(\mathbf{y})$ .

### 3 Stochastic differential equation mixed-effects models

As mentioned in the introduction, we may consider any generative model  $\mathcal{M}$  to describe time-dynamics in the data. We choose to provide illustrations based on models employing stochastic differential equations, however these could be substituted with other models, for example solvers for Markov jump processes for stochastic chemical reactions. Consider data from a population of  $M$  individuals. Assume that the dynamics for each individual  $i$  are described by a stochastic process  $\{\mathbf{X}_t^{(i)}\}_{t \geq 0}$  indexed by  $t$  (where  $t$  often indicates time though it can be something different as well), where  $\mathbf{X}_t^{(i)} \in \mathbb{R}^d$  for every  $t$  and every  $i = 1, \dots, M$ . Assume dynamics governed by the following stochastic differential equations (SDEs)

$$\begin{cases} d\mathbf{X}_t^{(i)} &= \boldsymbol{\mu}(\mathbf{X}_t, \mathbf{c}^{(i)}, \boldsymbol{\kappa}, t)dt + \boldsymbol{\sigma}(\mathbf{X}_t, \mathbf{c}^{(i)}, \boldsymbol{\kappa}, t)d\mathbf{B}_t^{(i)} \\ \mathbf{X}_0^{(i)} &= \mathbf{x}_0^{(i)} \quad i = 1, \dots, M, \\ \mathbf{c}^{(i)} &\sim \pi(\mathbf{c} | \boldsymbol{\eta}), \quad i = 1, \dots, M, \end{cases} \quad (1)$$

where  $\boldsymbol{\mu}$  is a  $d$ -dimensional drift vector, the diffusion coefficient  $\boldsymbol{\sigma}$  is a  $d \times d$  positive definite matrix, each  $\mathbf{B}_t^{(i)}$  denotes a vector of  $d$  independent

Wiener processes. In (1) we assume individual-specific parameters  $\mathbf{c}^{(i)} \in \mathbb{R}^q$ , while  $\boldsymbol{\kappa} \in \mathbb{R}^p$  is common to all individuals. For the individual-specific parameters we assume  $\mathbf{c}^{(i)} \sim \pi(\mathbf{c} | \boldsymbol{\eta})$  ( $i = 1, \dots, M$ ) and we denote their collection across all subjects as  $\mathbf{c} = (\mathbf{c}^{(1)}, \dots, \mathbf{c}^{(M)})$ . The parameter  $\boldsymbol{\eta}$  is called “population parameter” as it is underlying the distribution of all the  $\mathbf{c}^{(i)}$ , and as such it does not vary with  $i$ . Similarly, parameter  $\boldsymbol{\kappa}$  is also assumed not to vary with  $i$  and as such is common to all subjects, however, unlike  $\boldsymbol{\eta}$  for the  $\mathbf{c}^{(i)}$ ’s,  $\boldsymbol{\kappa}$  does not identify the distribution of any other random parameter.

The process  $\{\mathbf{X}_t^{(i)}\}$  may be observed directly (ie without error) or indirectly: here we consider the general observational model (2) where it is also possible to have noisy observations  $\mathbf{y}_t^{(i)}$  that are conditionally independent (given the latent process), and that are linked to  $\{\mathbf{X}_t^{(i)}\}$  via

$$\mathbf{Y}_t^{(i)} = g(\mathbf{X}_t^{(i)}, \boldsymbol{\varepsilon}_t^{(i)}), \quad \boldsymbol{\varepsilon}_t^{(i)} \sim \pi_{\varepsilon}(\boldsymbol{\xi}) \quad 1, \dots, M, \quad (2)$$

where  $\boldsymbol{\varepsilon}_t^{(i)}$  represents measurement errors with distribution  $\pi_{\varepsilon}(\boldsymbol{\xi})$  parameterised by the vector  $\boldsymbol{\xi} \in \mathbb{R}^s$ , and  $g(\cdot)$  is a (possibly non-linear) function. We exemplify the dependence relationship between the introduced parameters and the stochastic processes in Figure 1. Evidently, if we assume no measurement error, then the observations  $\mathbf{y}^{(i)}$  are direct (error-free) observations of  $\{\mathbf{X}_t^{(i)}\}_{t \geq 0}$ . Say that  $\mathbf{Y}_t^{(i)} \in \mathbb{R}^{d_o}$  where  $d_o \leq d$ , and that observations are collected at discrete time-points  $\{t_1, t_2, \dots, t_n\}$ , then we can have the case where at observational time  $t_j$  the observation  $\mathbf{y}_{t_j}^{(i)}$  is a vector of length  $d_o$  ( $j = 1, \dots, n$ ), where  $d_o = d$  corresponds to the system being fully observed at  $t_j$ , whereas having  $d_o < d$  opens up for  $\{\mathbf{X}_t^{(i)}\}$  being “partially observed”. A typical example would be  $\mathbf{Y}_{t_j}^{(i)} = \mathbf{F}_{t_j}^{(i)} \mathbf{X}_{t_j}^{(i)} + \boldsymbol{\varepsilon}_{t_j}^{(i)}$ , where the  $\mathbf{F}_{t_j}^{(i)}$  are  $d_o \times d$  matrices of known coefficients. In the notation introduced, we assumed for simplicity that the observational times are the same for all individuals, but we could have also used  $\{t_1^{(i)}, t_2^{(i)}, \dots, t_{n_i}^{(i)}\}$  and assumed that the set of observations are of different lengths  $n_i$  for different individuals: this can be handled in our framework but we decided to keep the notation lighter. The vector of observed data for subject  $i$  is therefore  $\mathbf{y}_o^{(i)} = (\mathbf{y}_{1,o}^{(i)}, \dots, \mathbf{y}_{n,o}^{(i)})$

where we used the shorthand  $\mathbf{y}_j^{(i)} \equiv \mathbf{y}_{t_j}^{(i)}$ . The full set of observations stacks all individual observations as  $\mathbf{y}_o = (\mathbf{y}_o^{(1)}, \dots, \mathbf{y}_o^{(M)})^\top$ . To simplify the reading, in next sections we will use  $\mathbf{y}$  to denote a generic dataset, observed or simulated, and we will distinguish the two cases only when necessary.

Equations (1)-(2) define a very flexible model, a *stochastic differential equation mixed-effects model* (SDEMEm), which is able to represent (i) stochastic intra-individual variation (via the diffusion terms in the SDEs), (ii) between individuals variation (via the distribution  $\pi(\mathbf{c}|\boldsymbol{\eta})$  of the individual parameters) and (iii) (optional) measurement variability (via  $\pi_\varepsilon(\boldsymbol{\xi})$ ), if measurement error is at all considered. Therefore, when measurement error is considered, (1)-(2) is a state-space model, because the latent process is Markovian and observations are assumed conditionally independent given the latent process. The Markovianity of  $\{\mathbf{X}_t^{(i)}\}_{t \geq 0}$  implies that, in principle, simulation of solution paths to SDEs could ideally arise via sampling  $\mathbf{x}_t^{(i)} \sim \pi(\mathbf{x}_t^{(i)}|\mathbf{x}_s^{(i)}, \cdot)$ , for any  $s < t$ , and  $\pi(\mathbf{x}_t^{(i)}|\mathbf{x}_s^{(i)}, \cdot)$  is the “transition density” of  $\{\mathbf{X}_t^{(i)}\}_{t \geq 0}$ . However, typically, and except for the simplest cases, we cannot solve the SDEs in equation (1) analytically, and transition densities are unavailable. Instead numerical approximations (schemes) are implemented. Here we consider the simplest possible approximation scheme, which is the Euler-Maruyama scheme, where the solution  $\mathbf{x}_t^{(i)}$  at time  $t$  is advanced to time  $t + \Delta_t$  via

$$\begin{aligned} \mathbf{x}_{t+\Delta_t}^{(i)} &= \mathbf{x}_t^{(i)} + \boldsymbol{\mu}(\mathbf{x}_t^{(i)}, \mathbf{c}^{(i)}, \boldsymbol{\kappa}, t) \Delta_t \\ &\quad + \boldsymbol{\sigma}(\mathbf{x}_t^{(i)}, \mathbf{c}^{(i)}, \boldsymbol{\kappa}, t) \cdot \mathbf{u}_t^{(i)}, \end{aligned} \quad (3)$$

where  $\mathbf{u}_t^{(i)} \sim \mathcal{N}(0, \Delta_t \mathbf{I}^{d \times d})$ , for some step size  $\Delta_t > 0$  and conditionally on  $\mathbf{c}^{(i)}$  and  $\boldsymbol{\kappa}$ . However, whenever possible, more accurate numerical scheme should be considered for the solution of (1) (a recent monography is [Higham and Kloeden 2021](#)), for example [Buckwar et al. \(2020\)](#) show the inference bias in the posterior of the parameters when certain SDEs are solved using Euler-Maruyama. In conclusion, the generative model that in Section 1 was denoted  $\mathcal{M}(\boldsymbol{\theta})$ , here it would ideally be the pair (1)-(2), however in practice it is a model that we could denote instead  $\mathcal{M}_\Delta(\boldsymbol{\theta})$ , since a numerical scheme with stepsize  $\Delta$

is required to solve the SDE, but we will keep writing  $\mathcal{M}(\boldsymbol{\theta})$  for simplicity. Importantly, while the applications and case-studies in this work focus on inference for SDE mixed-effects models where observations arise from a state-space model formulation (1)-(2), this is only a possible example of application of the methodology offered in Sections 5-6. In fact, the presented methodology named SeMPLE can be applied to *any* generative model  $\mathcal{M}(\boldsymbol{\theta})$ , and as such could even accommodate, for example, observations where the underlying processes  $\{X_t^{(i)}\}_{t \geq 0}$  are non-Markovian, or where the  $Y_t^{(i)}|X_t^{(i)}$  are not conditionally independent.

## 4 Bayesian inference for SDEMEmS

As mentioned in the previous section, we will use  $\mathbf{y}$  to denote both simulated data and observed data, and we will make use of the notation  $\mathbf{y}_o$  for observed data only when necessary. Denoting with  $\mathbf{y} = (\mathbf{y}^{(1)}, \dots, \mathbf{y}^{(M)})^\top$  the stacked data from all  $M$  individuals, the full vector of parameters to learn is  $\boldsymbol{\theta} = (\mathbf{c}, \boldsymbol{\kappa}, \boldsymbol{\eta}, \boldsymbol{\xi})$ , where  $\mathbf{c} = (\mathbf{c}^{(1)}, \dots, \mathbf{c}^{(M)})$ . Notice, if data are not assumed to be affected with measurement error, then  $\boldsymbol{\xi}$  would not appear in  $\boldsymbol{\theta}$ . Below we consider the most general scenario. Assume that the  $\mathbf{c}^{(i)}$ ’s are mutually independent and that data  $\mathbf{y}^{(i)}$  are independent conditionally on the  $\mathbf{c}^{(i)}$ ’s. We wish to sample from the full posterior distribution

$$\begin{aligned} \pi(\mathbf{c}, \boldsymbol{\kappa}, \boldsymbol{\eta}, \boldsymbol{\xi} | \mathbf{y}) &\propto \\ \pi(\boldsymbol{\kappa}, \boldsymbol{\eta}, \boldsymbol{\xi}) &\prod_{i=1}^M \pi(\mathbf{y}^{(i)} | \mathbf{c}^{(i)}, \boldsymbol{\kappa}, \boldsymbol{\xi}) \pi(\mathbf{c}^{(i)} | \boldsymbol{\eta}), \end{aligned} \quad (4)$$

where the individual likelihoods are obtained by the marginalization

$$\pi(\mathbf{y}^{(i)} | \mathbf{c}^{(i)}, \boldsymbol{\kappa}, \boldsymbol{\xi}) = \int \pi(\mathbf{y}^{(i)}, \mathbf{x}^{(i)} | \mathbf{c}^{(i)}, \boldsymbol{\kappa}, \boldsymbol{\xi}) d\mathbf{x}^{(i)} \quad (5)$$

$$\begin{aligned} &= \int \prod_{j=1}^{n_i} \pi(\mathbf{y}_j^{(i)} | \mathbf{x}_j^{(i)}, \boldsymbol{\xi}) \pi(\mathbf{x}_0^{(i)} | \mathbf{c}^{(i)}, \boldsymbol{\kappa}) \times \\ &\quad \prod_{j=1}^{n_i} \pi(\mathbf{x}_j^{(i)} | \mathbf{x}_{j-1}^{(i)}, \mathbf{c}^{(i)}, \boldsymbol{\kappa}) d\mathbf{x}_0^{(i)} \dots d\mathbf{x}_{n_i}^{(i)}, \end{aligned} \quad (6)$$



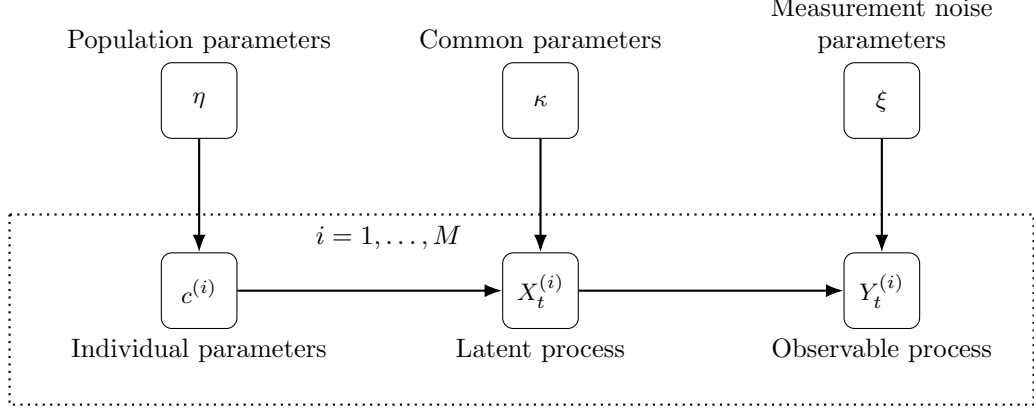


Fig. 1: Bayesian network model structure for a SDE mixed-effects model.

where the  $\mathbf{x}_j^{(i)} \equiv \mathbf{x}_{t_j}^{(i)}$  are values of the  $\{\mathbf{X}_t^{(i)}\}_{t \geq 0}$  process at the observational times, and where  $\mathbf{x}_0^{(i)}$  is a starting value for  $\{\mathbf{X}_t^{(i)}\}_{t \geq 0}$  at time  $t = 0$ . The integral (6) is generally analytically intractable, except for simple cases, which motivates the need for either particle methods (sequential Monte Carlo) to get an unbiased estimate of the individual likelihood or, as we propose, a simulation-based method that provides a deterministic surrogate model as an approximation of the individual likelihood.

We find that it is convenient to break down the sampling from (4) into smaller dimensional pieces by using a Gibbs sampler with the following three steps (Wiqvist et al. 2021; Persson et al. 2022)

$$\text{step 1: } \pi(\mathbf{c} | \boldsymbol{\kappa}, \boldsymbol{\eta}, \boldsymbol{\xi}, \mathbf{y}) \propto \prod_{i=1}^M \pi(\mathbf{c}^{(i)} | \boldsymbol{\eta}) \pi(\mathbf{y}^{(i)} | \mathbf{c}^{(i)}, \boldsymbol{\kappa}, \boldsymbol{\xi}) \quad (7)$$

$$\text{step 2: } \pi(\boldsymbol{\kappa}, \boldsymbol{\xi} | \mathbf{c}, \boldsymbol{\eta}, \mathbf{y}) \propto \pi(\boldsymbol{\kappa}, \boldsymbol{\xi}) \prod_{i=1}^M \pi(\mathbf{y}^{(i)} | \mathbf{c}^{(i)}, \boldsymbol{\kappa}, \boldsymbol{\xi}) \quad (8)$$

$$\text{step 3: } \pi(\boldsymbol{\eta} | \mathbf{c}, \boldsymbol{\kappa}, \boldsymbol{\xi}, \mathbf{y}) \propto \pi(\boldsymbol{\eta}) \prod_{i=1}^M \pi(\mathbf{c}^{(i)} | \boldsymbol{\eta}). \quad (9)$$

Notice that the first step (equation (7)) is equivalent to (10), which in practice we employ in our implementation. That is, since we assume that data from each individual  $i$  are conditionally independent from the data of another individual  $i'$  ( $i' \neq i$ ), then we can separately sample each individual  $\mathbf{c}^{(i)}$  ( $i = 1, \dots, M$ ) from

$$\pi(\mathbf{c}^{(i)} | \boldsymbol{\kappa}, \boldsymbol{\eta}, \boldsymbol{\xi}, \mathbf{y}^{(i)}) \propto \pi(\mathbf{c}^{(i)} | \boldsymbol{\eta}) \pi(\mathbf{y}^{(i)} | \mathbf{c}^{(i)}, \boldsymbol{\kappa}, \boldsymbol{\xi}), \quad (10)$$

then stack the obtained draws into  $\mathbf{c}$ . The fact that the first step is broken-down into  $M$  independent contributions allows for parallelization, and in case of a large number of individuals this could reduce the runtime significantly. The second step in the Gibbs sampler allows the fixed effects  $\boldsymbol{\kappa}$  and  $\boldsymbol{\xi}$  to be treated as parameters that are truly shared by all individuals: this is different from, for example, Arruda et al. (2024) where such shared parameters are assigned an arbitrarily chosen fixed variance and then treated as parameters that vary slightly between individuals. A good reason for considering a Gibbs sampler is that its first step (7) (or equivalently (10)), which requires a Metropolis-within-Gibbs approach, can benefit from an automatically learned proposal sampler that is particularly suited for multimodal targets, as we detail in Section 5. However, in practice, sampling from (7)-(8) when dealing with SDEMEMs is difficult, in that the individual likelihoods  $\pi(\mathbf{y}^{(i)} | \mathbf{c}^{(i)}, \boldsymbol{\kappa}, \boldsymbol{\xi})$  are typically intractable large-dimensional integrals (see (6)) that get approximated via Monte Carlo simulations, and we refer to Wiqvist et al. (2019), Botha et al. (2021) and Persson et al. (2022) for powerful but computer intensive approaches based on particle filters. Even worse, these computationally intensive Monte Carlo approximations, resulting in pseudomarginal pMCMC methods, are difficult to tune and have to be re-executed for any considered  $\boldsymbol{\theta}$  and whenever a new  $\mathbf{y}^{(i)}$  is considered. Hence large values of individuals ( $M$ ) can break down the feasibility of such approaches (but see the ameliorating strategies in Persson et al. 2022). To address this problem, in the next section, we

show how to obtain both an amortized surrogate likelihood model, and an amortized surrogate posterior model in the form of two Gaussian mixture models (“mixture of experts”). Moreover, we anticipate that there can be computational advantages in eliminating the second Gibbs step (hence assuming that all parameters are random effects), which is discussed in Section 6.1.

## 5 Likelihood and posterior estimation via mixtures of experts

The main contribution of this work is to create a framework for Bayesian inference where the likelihood  $\pi(\mathbf{y}|\mathbf{c}, \boldsymbol{\kappa}, \boldsymbol{\xi})$  is first approximated in an amortized way and then is specialized to a given observation  $\mathbf{y}_o^{(i)}$  (for every  $i = 1, \dots, M$ ). We say that our method is “semi-amortized” because, unlike amortized procedures, we do not simply plug the observation  $\mathbf{y}_o^{(i)}$  into an amortized approximation of  $\pi(\mathbf{y}|\mathbf{c}, \boldsymbol{\kappa}, \boldsymbol{\xi})$  that can be evaluated, but instead start from an amortized likelihood, and this is sequentially refined for the specific observation  $\mathbf{y}_o^{(i)}$ , to provide the final  $\pi(\mathbf{y}_o^{(i)}|\mathbf{c}, \boldsymbol{\kappa}, \boldsymbol{\xi})$ . We will see that the same computations involved in producing the approximation to  $\pi(\mathbf{y}_o^{(i)}|\mathbf{c}^{(i)}, \boldsymbol{\kappa}, \boldsymbol{\xi})$  will return, as a by-product and without any further computation, an approximation to the posterior  $\pi(\mathbf{c}^{(i)}, \boldsymbol{\kappa}, \boldsymbol{\xi}|\mathbf{y}_o^{(i)})$ . This is achieved via the *Sequential Mixtures Posterior and Likelihood Estimation* (SeMPLE) inference method of Häggström et al. (2024). Once all individual likelihoods  $\pi(\mathbf{y}_o^i|\mathbf{c}, \boldsymbol{\kappa}, \boldsymbol{\xi})$  are approximated with *deterministic* surrogate functions, they are used in place of intractable likelihoods in (7) and (8). This is different from the approach in Wiqvist et al. (2021), Botha et al. (2021) and Persson et al. (2022) that uses particle filters to compute (unbiased) Monte Carlo estimates of the likelihoods  $\pi(\mathbf{y}^{(i)}|\mathbf{c}^{(i)}, \boldsymbol{\kappa}, \boldsymbol{\xi})$ . It is of interest to investigate whether the surrogate likelihoods from SeMPLE provide accurate approximations of the true intractable likelihood and, thus, accurate posterior inference. It is also of interest to discuss the computational footprint of using SeMPLE to estimate the likelihoods compared to alternative methods such as Persson et al. (2022), Wiqvist et al. (2021) and Arruda et al. (2024).

The remaining of this section is not specific for stochastic mixed effects models, and here we use  $\mathbf{y}$  to denote a generic observable. SeMPLE uses surrogates that are mixture-of-experts whose parameters are fitted via expectation-maximization (Xu et al. 1994) on training data obtained via Markov chain Monte Carlo (MCMC). The SeMPLE approach makes repeated use, in a sequential way, of Gaussian locally linear mappings (GLLiM, Deleforge et al. 2014). GLLiM introduces a mixture of experts in the form of a Gaussian mixture model defined on the joint distribution for  $(\boldsymbol{\theta}, \mathbf{y})$ . The relationship between  $\mathbf{y} \in \mathbb{R}^{d_o \times n}$  and  $\boldsymbol{\theta} \in \mathbb{R}^l$  is assumed to be locally linear, defined using a latent variable  $z \in \{1, \dots, K\}$ , via the following *surrogate generative model*

$$\mathbf{y} = \sum_{k=1}^K \mathbb{I}_{\{z=k\}} (\tilde{\mathbf{A}}_k \boldsymbol{\theta} + \tilde{\mathbf{b}}_k + \tilde{\boldsymbol{\epsilon}}_k), \quad (11)$$

where  $\mathbb{I}$  denotes the indicator function, and  $\tilde{\mathbf{A}}_k \in \mathbb{R}^{(d_o \times n) \times l}$  and  $\tilde{\mathbf{b}}_k \in \mathbb{R}^{d_o \times n}$  are matrices and vectors, respectively, defining the affine transformation of  $\boldsymbol{\theta}$  in (11), while  $\tilde{\boldsymbol{\epsilon}}_k \in \mathbb{R}^{d_o \times n}$  corresponds to an error term capturing both the observational noise and the modelling error due to assuming an affine approximation for the data. In the following we consider Gaussian noise,  $\tilde{\boldsymbol{\epsilon}}_k \sim \mathcal{N}_{(d_o \times n)}(\mathbf{0}, \tilde{\boldsymbol{\Sigma}}_k)$ , and assume  $\tilde{\boldsymbol{\epsilon}}_k$  to not depend on  $\boldsymbol{\theta}$ ,  $\mathbf{y}$  nor  $z$ .

Conditionally on component  $z = k$ , an approximate generative model is given by

$$q_{\tilde{\boldsymbol{\phi}}}(\mathbf{y}|\boldsymbol{\theta}, z = k) = \mathcal{N}_{(d_o \times n)}(\mathbf{y}; \tilde{\mathbf{A}}_k \boldsymbol{\theta} + \tilde{\mathbf{b}}_k, \tilde{\boldsymbol{\Sigma}}_k). \quad (12)$$

To complete the hierarchical model,  $\boldsymbol{\theta}$  is assumed to follow a mixture of Gaussian distributions specified by

$$q_{\tilde{\boldsymbol{\phi}}}(\boldsymbol{\theta}|z = k) = \mathcal{N}_l(\boldsymbol{\theta}; \tilde{\mathbf{c}}_k, \tilde{\boldsymbol{\Gamma}}_k), \quad q_{\tilde{\boldsymbol{\phi}}}(z = k) = \pi_k. \quad (13)$$

The GLLiM hierarchical construction above (eq.(11) to (13)) defines a joint Gaussian mixture model on  $(\mathbf{y}, \boldsymbol{\theta})$ :

$$q_{\tilde{\boldsymbol{\phi}}}(\mathbf{y}, \boldsymbol{\theta}) = \sum_{k=1}^K q_{\tilde{\boldsymbol{\phi}}}(\mathbf{y}|\boldsymbol{\theta}, z = k) q_{\tilde{\boldsymbol{\phi}}}(\boldsymbol{\theta}|z = k) q_{\tilde{\boldsymbol{\phi}}}(z = k),$$

where the full vector of mixture model parameters is  $\tilde{\boldsymbol{\phi}} = \{\pi_k, \tilde{\mathbf{c}}_k, \tilde{\boldsymbol{\Gamma}}_k, \tilde{\mathbf{A}}_k, \tilde{\mathbf{b}}_k, \tilde{\boldsymbol{\Sigma}}_k\}_{k=1}^K$ . Given this joint distribution, we can easily deduce the

conditional distributions  $q_{\tilde{\phi}}(\mathbf{y} | \boldsymbol{\theta})$  and  $q_{\phi}(\boldsymbol{\theta} | \mathbf{y})$  in closed-form. First, we have the surrogate likelihood

$$q_{\tilde{\phi}}(\mathbf{y} | \boldsymbol{\theta}) = \sum_{k=1}^K \tilde{\eta}_k(\boldsymbol{\theta}) \mathcal{N}_{(d_o \times n)}(\mathbf{y}; \tilde{\mathbf{A}}_k \boldsymbol{\theta} + \tilde{\mathbf{b}}_k, \tilde{\boldsymbol{\Sigma}}_k), \quad (14)$$

with

$$\tilde{\eta}_k(\boldsymbol{\theta}) = \frac{\pi_k \mathcal{N}_l(\boldsymbol{\theta}; \tilde{\mathbf{c}}_k, \tilde{\boldsymbol{\Gamma}}_k)}{\sum_{j=1}^K \pi_j \mathcal{N}_l(\boldsymbol{\theta}; \tilde{\mathbf{c}}_j, \tilde{\boldsymbol{\Gamma}}_j)}. \quad (15)$$

Notice the important distinction that  $q_{\tilde{\phi}}(\mathbf{y} | \boldsymbol{\theta})$  is the approximate (surrogate) likelihood, while  $\pi(\mathbf{y} | \boldsymbol{\theta})$  is the true (unknown) likelihood that underlines the generative model that we denoted with  $\mathcal{M}(\boldsymbol{\theta})$  in Section 1 and that, for SDEMEmS, corresponds to equations (1)-(2). Remarkably, we instantaneously also obtain a surrogate posterior

$$q_{\phi}(\boldsymbol{\theta} | \mathbf{y}) = \sum_{k=1}^K \eta_k(\mathbf{y}) \mathcal{N}_l(\boldsymbol{\theta}; \mathbf{A}_k \mathbf{y} + \mathbf{b}_k, \boldsymbol{\Sigma}_k), \quad (16)$$

with

$$\eta_k(\mathbf{y}) = \frac{\pi_k \mathcal{N}_{(d_o \times n)}(\mathbf{y}; \mathbf{c}_k, \boldsymbol{\Gamma}_k)}{\sum_{j=1}^K \pi_j \mathcal{N}_{(d_o \times n)}(\mathbf{y}; \mathbf{c}_j, \boldsymbol{\Gamma}_j)}, \quad (17)$$

where  $\phi = \{\pi_k, \mathbf{c}_k, \boldsymbol{\Gamma}_k, \mathbf{A}_k, \mathbf{b}_k, \boldsymbol{\Sigma}_k\}_{k=1}^K$ . The surrogate (16) is obtained instantaneously and in closed-form, because we have the following algebraic relationships deduced from  $\tilde{\phi}$  (Deleforge et al. 2014):

$$\mathbf{c}_k = \tilde{\mathbf{A}}_k \tilde{\mathbf{c}}_k + \tilde{\mathbf{b}}_k, \quad (18)$$

$$\boldsymbol{\Gamma}_k = \tilde{\boldsymbol{\Sigma}}_k + \tilde{\mathbf{A}}_k \tilde{\boldsymbol{\Gamma}}_k \tilde{\mathbf{A}}_k^{\top}, \quad (19)$$

$$\boldsymbol{\Sigma}_k = (\tilde{\boldsymbol{\Gamma}}_k^{-1} + \tilde{\mathbf{A}}_k^{\top} \tilde{\boldsymbol{\Sigma}}_k^{-1} \tilde{\mathbf{A}}_k)^{-1}, \quad (20)$$

$$\mathbf{A}_k = \boldsymbol{\Sigma}_k \tilde{\mathbf{A}}_k^{\top} \tilde{\boldsymbol{\Sigma}}_k^{-1}, \quad (21)$$

$$\mathbf{b}_k = \boldsymbol{\Sigma}_k (\tilde{\boldsymbol{\Gamma}}_k^{-1} \tilde{\mathbf{c}}_k - \tilde{\mathbf{A}}_k^{\top} \tilde{\boldsymbol{\Sigma}}_k^{-1} \tilde{\mathbf{b}}_k). \quad (22)$$

Therefore, given training data of model parameters and simulated data  $\{\boldsymbol{\theta}_n, \mathbf{y}_n\}_{n=1}^N$ ,  $\tilde{\phi}$  is first estimated via expectation-maximization (EM, Deleforge et al. 2014), to produce  $q_{\tilde{\phi}}(\mathbf{y} | \boldsymbol{\theta})$ , and then the corresponding approximation for  $\phi$  is obtained at no cost via (18)–(22), so that the surrogate posterior  $q_{\phi}(\boldsymbol{\theta} | \mathbf{y})$  is also identified. To run EM, our implementation of SeMPLE uses the R xLLiM package (Perthame et al. 2022), which

gives several options to parametrize the covariance matrices  $\tilde{\boldsymbol{\Sigma}}_k$  (and hence, implicitly, also the  $\boldsymbol{\Sigma}_k$ ), see Appendix B for more details. Before moving forward, notice that the number of components  $K$  used either in (14) or (16) can be set in a principled way, as described in Appendix B, where the Bayesian information criterion (BIC) is employed. Moreover, in Section 6 we discuss how a starting value of  $K$  (determined via BIC) is let decrease dynamically during a run of the inference algorithm, thus drastically reducing the number of parameters  $\tilde{\phi}$  (and hence  $\phi$ ) to determine.

Rewriting the Gibbs sampler in equations (7)–(9) with the surrogate likelihood  $q_{\tilde{\phi}}$  results in the following approximated Gibbs steps (the third step is still exact as it does not involve likelihoods)

$$\hat{\pi}(\mathbf{c}^{(i)} | \boldsymbol{\kappa}, \boldsymbol{\eta}, \boldsymbol{\xi}, \mathbf{y}^{(i)}) \propto \pi(\mathbf{c}^{(i)} | \boldsymbol{\eta}) q_{\tilde{\phi}}(\mathbf{y}^{(i)} | \mathbf{c}^{(i)}, \boldsymbol{\kappa}, \boldsymbol{\xi}), \quad (23)$$

$$i = 1, \dots, M.$$

$$\hat{\pi}(\boldsymbol{\kappa}, \boldsymbol{\xi} | \mathbf{c}, \boldsymbol{\eta}, \mathbf{y}) \propto \pi(\boldsymbol{\kappa}, \boldsymbol{\xi}) \prod_{i=1}^M q_{\tilde{\phi}}(\mathbf{y}^{(i)} | \mathbf{c}^{(i)}, \boldsymbol{\kappa}, \boldsymbol{\xi}) \quad (24)$$

$$\pi(\boldsymbol{\eta} | \mathbf{c}, \boldsymbol{\kappa}, \boldsymbol{\xi}, \mathbf{y}) \propto \pi(\boldsymbol{\eta}) \prod_{i=1}^M \pi(\mathbf{c}^{(i)} | \boldsymbol{\eta}). \quad (25)$$

Note that, in terms of the GLLiM notation, we have  $\boldsymbol{\theta} = (\mathbf{c}, \boldsymbol{\kappa}, \boldsymbol{\xi})$  rather than  $\boldsymbol{\theta} = (\mathbf{c}, \boldsymbol{\kappa}, \boldsymbol{\eta}, \boldsymbol{\xi})$ , and this is because, since the third Gibbs step does not involve likelihoods, GLLiM is not used to infer  $\boldsymbol{\eta}$ , given that  $\boldsymbol{\eta}$  can be sampled in (25) in an exact way, either via conjugacy or using of-the-shelves algorithms such as Hamiltonian Monte Carlo (HMC). As the surrogate likelihood provided by GLLiM is a mixture of Gaussians, this is differentiable, and therefore, it is possible to use gradient-informed MCMC methods such as HMC. This is an advantage compared to the previously mentioned pseudo-marginal methods that provide non-differentiable estimates of the intractable likelihood, often involving manual tuning for the initialization of the proposal distribution covariance matrices needed in random walk Metropolis-Hastings. However, as we motivate in Section 6, we will prefer to employ  $q_{\phi}(\boldsymbol{\theta} | \mathbf{y})$  as a multimodal proposal sampler in step 1 (eq. (23)), and instead employ HMC only for the other two steps. Furthermore, in Section 6.1, we illustrate another,



more scalable, Gibbs sampler associated to assuming all parameters as random effects. To efficiently apply this sampler with the surrogate likelihood, we first train the GLLiM model on simulated data in a sequential manner, ensuring that the data become increasingly informative for the observed  $\mathbf{y}_o$ . The full procedure is described in the SeMPLE mixed-effects algorithm in the following section.

## 6 SeMPLE for mixed-effects models

The SeMPLE inference scheme for mixed-effects models is described in Algorithm 1, and it repeatedly applies the GLLiM approach (introduced in Section 5) across  $R$  “rounds”, using a set of increasingly more informative training data. We will see that the  $R$  rounds provide increasingly accurate surrogate likelihood and surrogate posteriors which are initially amortized, and then become specialized to the specific observed data  $\mathbf{y}_o$ . At first, in round  $r = 0$ , an initial batch of  $N$  tuples  $\mathcal{D}_0 = \{(\mathbf{c}_j, \boldsymbol{\kappa}_j, \boldsymbol{\xi}_j), \mathbf{y}^{(j)}\}_{j=1}^N$  are produced from the prior-predictive distributions (steps 1-4 of Algorithm 1). Notice, here each  $\mathbf{y}^{(j)}$  does not have the same dimension of  $\mathbf{y}_o = \{\mathbf{y}_o^{(i)}\}_{i=1}^M$ , that is, it is not a collection of  $M$  simulated individual datasets, but is instead an individual simulated trajectory. This data set  $\mathcal{D}_0$  constitutes the initial training data for GLLiM, and the mixture model parameters  $\tilde{\phi}_0$  and  $\phi_0$  are obtained via EM within GLLiM to produce the initial *amortized* surrogate likelihood and posterior  $q_{\tilde{\phi}_0}(\mathbf{y} | \mathbf{c}, \boldsymbol{\kappa}, \boldsymbol{\xi})$  and  $q_{\phi_0}(\mathbf{c}, \boldsymbol{\kappa}, \boldsymbol{\xi} | \mathbf{y})$  respectively (steps 6-7 of Algorithm 1). The number of mixture components  $K$  in the surrogate likelihood and surrogate posterior is allowed to decrease between the SeMPLE’s rounds, as denoted by “*update K*” in steps 7, 14 and 25. How this is done is discussed in Section 6.2, but shortly,  $K$  is reduced in a principled way to prevent having too many irrelevant mixture components, whose parameters may be difficult to identify as hardly appearing in the training data, but also to drastically reduce the number of components of  $\tilde{\phi}$  and  $\phi$  to determine. This concludes round  $r = 0$  of SeMPLE.

Next comes round  $r = 1$ , where steps 9-10 aim to refine the initial amortized surrogate models by utilizing the observed data  $\mathbf{y}_o = (\mathbf{y}_o^{(1)}, \dots, \mathbf{y}_o^{(M)})$ .

This is done by sampling  $N_s$  times (which generally need not be as large as the prior predictive size  $N$  but rather  $N_s < N$ ) from the learned amortized posterior (which is a Gaussian mixture model) by first inputting  $\mathbf{y}^{(i)} \leftarrow \mathbf{y}_o^{(i)}$  inside  $q_{\phi_0}(\mathbf{c}, \boldsymbol{\kappa}, \boldsymbol{\xi} | \mathbf{y}^{(i)})$ , and then sampling  $(\mathbf{c}_j^{(i)}, \boldsymbol{\kappa}_j^{(i)}, \boldsymbol{\xi}_j^{(i)}) \sim q_{\phi_0}(\mathbf{c}, \boldsymbol{\kappa}, \boldsymbol{\xi} | \mathbf{y}_o^{(i)})$  (step 9), which is trivial to do, and then conditionally on each of the  $N_s$  posterior draws in step 10 we produce a corresponding simulated observation  $\mathbf{y}_j^{(i)} \sim p(\mathbf{y} | \mathbf{c}_j^{(i)}, \boldsymbol{\kappa}_j^{(i)}, \boldsymbol{\xi}_j^{(i)})$  (implicitly from the computer simulator for (2)). Note that we use the notation  $\boldsymbol{\kappa}_j^{(i)}$  and  $\boldsymbol{\xi}_j^{(i)}$  to emphasize that the shared parameters  $\boldsymbol{\kappa}$  and  $\boldsymbol{\xi}$  are sampled from the surrogate posterior conditional on  $\mathbf{y}_o^{(i)}$ . Hence,  $\boldsymbol{\kappa}_j^{(i)}$  and  $\boldsymbol{\xi}_j^{(i)}$  depend only on the observation  $\mathbf{y}_o^{(i)}$  and not on all  $M$  individuals in the data  $\mathbf{y}_o$ . The surrogate posterior samples and the simulated observations are then collected into a new training data set  $\mathcal{D}_1^i = \{(\mathbf{c}_j^{(i)}, \boldsymbol{\kappa}_j^{(i)}, \boldsymbol{\xi}_j^{(i)}), \mathbf{y}_j^{(i)}\}_{j=1}^{N_s}$ . This is repeated for each individual  $i$  and GLLiM is then trained on the union of training data sets from all individuals  $\mathcal{D}_1 = \bigcup_{i=1}^M \mathcal{D}_1^i$  to get new estimators  $\tilde{\phi}_1$  and  $\phi_1$  and hence data-informed surrogate likelihood and posterior (steps 13-14), which concludes round  $r = 1$ . Notice that it is possible for samples from the initial surrogate  $(\mathbf{c}_j^{(i)}, \boldsymbol{\kappa}_j^{(i)}, \boldsymbol{\xi}_j^{(i)}) \sim q_{\phi_0}(\mathbf{c}, \boldsymbol{\kappa}, \boldsymbol{\xi} | \mathbf{y}_o^{(i)})$  to “leak” outside of the prior’s support, if this is bounded (the leaking is not possible in later steps where a Metropolis-Hastings regularization is implemented), therefore step 9 in Algorithm 1 could also be written to include a rejection procedure whenever  $\pi(\mathbf{c}_j^{(i)}, \boldsymbol{\kappa}_j^{(i)}, \boldsymbol{\xi}_j^{(i)}) = 0$ , so that the sampling is repeated until  $N_s$  parameters having  $\pi(\mathbf{c}_j^{(i)}, \boldsymbol{\kappa}_j^{(i)}, \boldsymbol{\xi}_j^{(i)}) > 0$  are collected.

After initializing  $\mathbf{c}, \boldsymbol{\kappa}, \boldsymbol{\xi}$  and  $\boldsymbol{\eta}$  (step 15), the remaining part of the algorithm concerns producing  $N_g$  samples from the Gibbs steps in eq. (23)-(25), by utilizing the surrogate likelihood  $q_{\tilde{\phi}_1}(\mathbf{y} | \mathbf{c}, \boldsymbol{\kappa}, \boldsymbol{\xi})$  and posterior  $q_{\phi_1}(\mathbf{c}, \boldsymbol{\kappa}, \boldsymbol{\xi} | \mathbf{y})$ . First, the individual parameters  $\mathbf{c}^{(i)}$  in (23) are sampled for subject  $i$  independently of other subjects (step 18) according to an independence-Metropolis-Hastings algorithm (Robert and Casella 2004) detailed in Algorithm 2 and that we justify further below. Note that the surrogate posterior  $q_{\phi}(\mathbf{c} | \mathbf{y}_o^{(i)})$ , where the components corresponding to  $\boldsymbol{\kappa}$  and  $\boldsymbol{\xi}$  have been removed, is being used as

---

**Algorithm 1** SeMPLE for mixed-effects models
 

---

**Input:**  $\pi(\mathbf{c}|\boldsymbol{\eta})$ ,  $\pi(\boldsymbol{\eta})$ ,  $\pi(\boldsymbol{\kappa}, \boldsymbol{\xi})$ , observed data  $\{\mathbf{y}_o^{(i)}\}_{i=1}^M$ , simulator  $\pi(\mathbf{y}|\mathbf{c}, \boldsymbol{\kappa}, \boldsymbol{\xi})$ , positive integers  $R$  (number of SeMPLE rounds),  $N$  (number of prior predictive simulations at round  $r = 0$ ),  $N_s$  (number of simulations per individual at round  $r = 1$ ),  $N_g$  (number of Gibbs samples),  $N_{MH}$  (number of Metropolis-Hastings iterations).

**Output:** Posterior samples  $\{\{\mathbf{c}_j^{(i)}\}_{i=1}^M, \boldsymbol{\kappa}_j, \boldsymbol{\xi}_j, \boldsymbol{\eta}_j\}_{j=1}^{N_g}$

- 1: Sample iid  $\boldsymbol{\eta}_j \sim \pi(\boldsymbol{\eta})$ ,  $j = 1, \dots, N$
  - 2: Sample  $\mathbf{c}_j \sim \pi(\mathbf{c}|\boldsymbol{\eta}_j)$ ,  $j = 1, \dots, N$
  - 3: Sample  $(\boldsymbol{\kappa}_j, \boldsymbol{\xi}_j) \sim \pi(\boldsymbol{\kappa}, \boldsymbol{\xi})$ ,  $j = 1, \dots, N$
  - 4: Simulate  $N$  single-individual datasets  $\mathbf{y}^{(j)} \sim \pi(\mathbf{y}|\mathbf{c}_j, \boldsymbol{\kappa}_j, \boldsymbol{\xi}_j)$ ,  $j = 1, \dots, N$
  - 5: Collect  $\mathcal{D}_0 = \{(\mathbf{c}_j, \boldsymbol{\kappa}_j, \boldsymbol{\xi}_j), \mathbf{y}^{(j)}\}_{j=1}^N$
  - 6: Train  $q_{\phi_0}(\mathbf{y}|\mathbf{c}, \boldsymbol{\kappa}, \boldsymbol{\xi})$  on  $\mathcal{D}_0$ .
  - 7: Obtain  $q_{\phi_0}(\mathbf{c}, \boldsymbol{\kappa}, \boldsymbol{\xi}|\mathbf{y})$ . Update  $K$
  
  - 8: **for**  $i = 1 : M$  **do**
  - 9:   Sample from surrogate posterior iid  $(\mathbf{c}_j^{(i)}, \boldsymbol{\kappa}_j^{(i)}, \boldsymbol{\xi}_j^{(i)}) \sim q_{\phi_0}(\mathbf{c}, \boldsymbol{\kappa}, \boldsymbol{\xi}|\mathbf{y}_o^{(i)})$ ,  $j = 1, \dots, N_s$
  - 10:   Simulate  $\mathbf{y}_j^{(i)} \sim \pi(\mathbf{y}|\mathbf{c}_j^{(i)}, \boldsymbol{\kappa}_j^{(i)}, \boldsymbol{\xi}_j^{(i)})$ ,  $j = 1, \dots, N_s$
  - 11:   Collect  $\mathcal{D}_1^i = \{(\mathbf{c}_j^{(i)}, \boldsymbol{\kappa}_j^{(i)}, \boldsymbol{\xi}_j^{(i)}), \mathbf{y}_j^{(i)}\}_{j=1}^{N_s}$
  - 12: **end for**
  - 13: Train  $q_{\phi_1}(\mathbf{y}|\mathbf{c}, \boldsymbol{\kappa}, \boldsymbol{\xi})$  on  $\mathcal{D}_1 = \bigcup_{i=1}^M \mathcal{D}_1^i$
  - 14: Obtain  $q_{\phi_1}(\mathbf{c}, \boldsymbol{\kappa}, \boldsymbol{\xi}|\mathbf{y})$ . Update  $K$
  
  - 15: Initialize  $\mathbf{c}_1 \leftarrow \mathbf{c}_{N_s}$ ,  $(\boldsymbol{\kappa}_1, \boldsymbol{\xi}_1) = (\bar{\boldsymbol{\kappa}}_{N_s}, \bar{\boldsymbol{\xi}}_{N_s})$ , and  $\boldsymbol{\eta}_1 \sim \pi(\boldsymbol{\eta})$
  - 16: **for**  $r = 2 : R$  **do**
  - 17:   **for**  $j = 2 : N_g$  **do**
  - 18:     Sample new  $\mathbf{c}_j^{(i)} \sim \pi(\mathbf{c}_{j-1}^{(i)}|\boldsymbol{\eta}_{j-1})q_{\phi_{r-1}}(\mathbf{y}_o^{(i)}|\mathbf{c}_{j-1}^{(i)}, \boldsymbol{\kappa}_{j-1}, \boldsymbol{\xi}_{j-1})$ ,  $i = 1, \dots, M$  via Algorithm 2
  - 19:     Sample new  $(\boldsymbol{\kappa}_j, \boldsymbol{\xi}_j) \sim \pi(\boldsymbol{\kappa}_{j-1}, \boldsymbol{\xi}_{j-1}) \prod_{i=1}^M q_{\phi_{r-1}}(\mathbf{y}_o^{(i)}|\mathbf{c}_j^{(i)}, \boldsymbol{\kappa}_{j-1}, \boldsymbol{\xi}_{j-1})$  via HMC
  - 20:     Sample new  $\boldsymbol{\eta}_j \sim \pi(\boldsymbol{\eta}_{j-1}) \prod_{i=1}^M \pi(\mathbf{c}_j^{(i)}|\boldsymbol{\eta}_{j-1})$  via HMC or conjugacy
  - 21:     Simulate  $\mathbf{y}_j^{(i)} \sim \pi(\mathbf{y}|\mathbf{c}_j^{(i)}, \boldsymbol{\kappa}_j, \boldsymbol{\xi}_j)$ ,  $i = 1, \dots, M$
  - 22:   **end for**
  - 23:   Collect  $\mathcal{D}_r = \left\{ \{\mathbf{c}_j^{(i)}\}_{i=1}^M, \boldsymbol{\kappa}_j, \boldsymbol{\xi}_j, \{\mathbf{y}_j^{(i)}\}_{i=1}^M \right\}_{j=1}^{N_g}$
  - 24:   Train  $q_{\phi_r}(\mathbf{y}|\mathbf{c}, \boldsymbol{\kappa}, \boldsymbol{\xi})$  on  $\bigcup_{\tilde{r}=1}^r \mathcal{D}_{\tilde{r}}$
  - 25:   Obtain  $q_{\phi_r}(\mathbf{c}, \boldsymbol{\kappa}, \boldsymbol{\xi}|\mathbf{y})$ . Update  $K$
  - 26: **end for**
- 

a *self-tuned* proposal distribution in Algorithm 2 (it is “self-tuned” because (i) the means and covariance matrices of its components have been automatically provided by the EM procedure, and (ii) it is conditional to the observed data  $\mathbf{y}_o^{(i)}$ ). Proposing independently from  $q_{\phi}(\cdot|\mathbf{y}_o^{(i)})$  is a key feature of SeMPLE: since this proposal function is a mixture model, it is particularly suited for the exploration of multimodal posteriors, and the fact that it has been derived from the same training data as for the surrogate likelihood (and has the same number of components as the mixture model of the likelihood) makes

it an appropriate proposal sampler. Moreover,  $q_{\phi}(\cdot|\mathbf{y}_o^{(i)})$  is conditional on the individual-specific  $\mathbf{y}_o^{(i)}$ , and this makes it particularly well-informed for the task of sampling specifically  $\mathbf{c}^{(i)}$  in (23). Next, in step 19,  $\boldsymbol{\kappa}$  and  $\boldsymbol{\xi}$  are updated by targeting the posterior proportional to  $\pi(\boldsymbol{\kappa}_{j-1}, \boldsymbol{\xi}_{j-1}) \prod_{i=1}^M q_{\phi_{r-1}}(\mathbf{y}_o^{(i)}|\mathbf{c}_j^{(i)}, \boldsymbol{\kappa}_{j-1}, \boldsymbol{\xi}_{j-1})$ , however here the sampling is instead carried out using HMC, and we justify this specific choice further below. To run HMC we use **Stan** (Stan Development Team 2023) through the interfaces **RStan** (Stan Development Team 2024) and **cmdstanr** (Gabry et al. 2024). The final step

---

**Algorithm 2** Independence-Metropolis-Hastings for  $\mathbf{c}$ 


---

```

1: Here round  $r$  is  $r \geq 2$  and  $q_{\phi_{r-1}}(\mathbf{c} | \mathbf{y}_o^{(i)})$  produces independent samples. For the initial value  $\tilde{\mathbf{c}}_1^{(i)}$ , pick the
   last accepted value  $\mathbf{c}_{j-1}^{(i)}$  from the currently available Markov chain produced in the previous Gibbs sample.
2: for  $l = 2 : N_{MH}$  do
3:   Propose  $\tilde{\mathbf{c}}_*^{(i)} \sim q_{\phi_{r-1}}(\mathbf{c} | \mathbf{y}_o^{(i)})$  independently,
4:    $\alpha = \min \left\{ 1, \frac{\pi(\tilde{\mathbf{c}}_*^{(i)} | \boldsymbol{\eta}_{j-1}) q_{\tilde{\phi}_{r-1}}(\mathbf{y}_o^{(i)} | \tilde{\mathbf{c}}_*^{(i)}, \boldsymbol{\kappa}_{j-1}, \boldsymbol{\xi}_{j-1})}{\pi(\tilde{\mathbf{c}}_{l-1}^{(i)} | \boldsymbol{\eta}_{j-1}) q_{\tilde{\phi}_{r-1}}(\mathbf{y}_o^{(i)} | \tilde{\mathbf{c}}_{l-1}^{(i)}, \boldsymbol{\kappa}_{j-1}, \boldsymbol{\xi}_{j-1})} \times \frac{q_{\phi_{r-1}}(\tilde{\mathbf{c}}_{l-1}^{(i)} | \mathbf{y}_o^{(i)})}{q_{\phi_{r-1}}(\tilde{\mathbf{c}}_*^{(i)} | \mathbf{y}_o^{(i)})} \right\}$ 
5:   Sample  $u \sim \mathcal{U}[0, 1]$ 
6:   if  $u \leq \alpha$  then
7:      $\tilde{\mathbf{c}}_l^{(i)} = \tilde{\mathbf{c}}_*^{(i)}$ 
8:   else
9:      $\tilde{\mathbf{c}}_l^{(i)} = \tilde{\mathbf{c}}_{l-1}^{(i)}$ 
10:  end if
11: end for
12:  $\mathbf{c}_j^{(i)} = \tilde{\mathbf{c}}_{N_{MH}}^{(i)}$ 

```

---

of the Gibbs sampler (step 20) does not involve surrogate likelihoods, and can therefore be easily dealt with using HMC, or can be sampled exactly by using Normal-Gamma conjugate priors, as detailed in Appendix A. We plug the newly obtained samples into the computer simulator for (2) to obtain  $\mathbf{y}_j^{(i)} \sim p(\mathbf{y} | \mathbf{c}_j^{(i)}, \boldsymbol{\kappa}_j, \boldsymbol{\xi}_j)$ ,  $i = 1, \dots, M$ . The procedure is then repeated to obtain  $N_g$  samples of each parameter and corresponding simulated observations. The Gibbs samples and corresponding simulated observations for all  $M$  individuals are collected into a data set  $\mathcal{D}_r = \left\{ \left\{ \mathbf{c}_j^{(i)} \right\}_{i=1}^M, \boldsymbol{\kappa}_j, \boldsymbol{\xi}_j, \left\{ \mathbf{y}_j^{(i)} \right\}_{i=1}^M \right\}_{j=1}^{N_g}$ , and GLLiM is then trained on all data sets up until this point  $\bigcup_{\tilde{r}=1}^r \mathcal{D}_{\tilde{r}}$  (with the exception of the prior-predictive data  $\mathcal{D}_0$  which is deemed too uninformative to refine surrogates for specific observed data), to obtain an updated surrogate likelihood and posterior  $q_{\tilde{\phi}_r}(\mathbf{y} | \mathbf{c}, \boldsymbol{\kappa}, \boldsymbol{\xi})$  and  $q_{\phi_r}(\mathbf{c}, \boldsymbol{\kappa}, \boldsymbol{\xi} | \mathbf{y})$  respectively (steps 24-25). The full Gibbs procedure is then repeated with the new surrogate likelihood and posterior until the final round  $R$  is reached. We do not recommend to consider  $R > 3$  rounds, and the results in our experiments are obtained with  $R = 2$  showing excellent mixing in the chains (see traceplots in the Supplementary Material). A number of rounds larger than three has diminishing returns, and could possibly produce training data that is potentially affected by more sticky chains, reducing the quality of the surrogate mixture models.

The reason for using HMC in step 19, instead of using the surrogate posterior  $q_{\phi}(\mathbf{c}^{(i)}, \boldsymbol{\kappa}, \boldsymbol{\xi} | \mathbf{y}_o^{(i)})$  as independence proposal distribution, is that when new values for  $\boldsymbol{\kappa}$  and  $\boldsymbol{\xi}$  are sampled, they need to be proposed conditional on all observations in  $\mathbf{y}_o = (\mathbf{y}_o^{(1)}, \dots, \mathbf{y}_o^{(M)})$ . This is not compatible with the individual surrogate posterior  $q_{\phi}(\mathbf{c}^{(i)}, \boldsymbol{\kappa}, \boldsymbol{\xi} | \mathbf{y}_o^{(i)})$  that we learn with SeMPLE, as each individual surrogate distribution depends only on the observation of one individual  $\mathbf{y}_o^{(i)}$ . To circumvent this, one would need to train an additional “global” surrogate model  $q_{\phi}(\mathbf{c}, \boldsymbol{\kappa}, \boldsymbol{\xi} | \mathbf{y}_o)$  that is conditional on the entire observed data set  $\mathbf{y}_o$ . However, for increasing  $M$ , the dimension of  $\mathbf{y}_o$  may become too large to fit a GLLiM model to “raw data” (ie non-summarized data) in this way. Hence, we use HMC to propose new values for  $\boldsymbol{\kappa}$  and  $\boldsymbol{\xi}$ . This problem may be relaxed if the inference was based not on the raw observed data, but on summary statistics thereof, and hence reduce the data-dimensionality problem as commonly done in approximate Bayesian computation literature. In Section 6.1 we illustrate an opportunity to obtain a much more scalable Gibbs sampler, that corresponds to a slightly different model formulation.

### 6.1 A scalable SeMPLE approach for mixed-effects models

The approach we have described thus far offers a compelling framework for Bayesian inference in

mixed-effects models by automatically constructing surrogate likelihoods and posteriors, including MCMC proposal samplers, that are both efficient to evaluate and fast to sample from. However, it is possible to obtain considerable gains in terms of computational scalability, by slightly reducing the generality of the mixed-effects model, namely not assume any shared parameters  $(\boldsymbol{\kappa}, \boldsymbol{\xi})$ , and instead allow these to become part of the individual parameters  $\mathbf{c}^{(i)}$ , and hence be random effects. This means that the second Gibbs step can be avoided. This approach is similar to the “perturbed” model in Persson et al. (2022); however, while they fixed the variance of certain parameters, we infer the population variance for all parameters. The three-steps Gibbs sampler (23)-(25) is replaced by the following two-steps Gibbs sampler

$$\text{step 1: } \hat{\pi}(\mathbf{c}^{(i)} | \boldsymbol{\eta}, \mathbf{y}^{(i)}) \propto \pi(\mathbf{c}^{(i)} | \boldsymbol{\eta}) q_{\tilde{\boldsymbol{\phi}}}(\mathbf{y}^{(i)} | \mathbf{c}^{(i)}), \quad (26)$$

$$i = 1, \dots, M.$$

$$\text{step 2: } \pi(\boldsymbol{\eta} | \mathbf{c}, \mathbf{y}) \propto \pi(\boldsymbol{\eta}) \prod_{i=1}^M \pi(\mathbf{c}^{(i)} | \boldsymbol{\eta}). \quad (27)$$

This “reduced” Gibbs sampler, where  $\mathbf{c}^{(i)} = (\dots, \boldsymbol{\kappa}^{(i)}, \boldsymbol{\xi}^{(i)})$ , has the potential to scale much better with the number of individuals in the data set. The reason why it is beneficial for scaling to remove the fixed-effects is two-fold. First, this removes the need to target the full likelihood  $\prod_{i=1}^M q_{\tilde{\boldsymbol{\phi}}}(\mathbf{y}^{(i)} | \mathbf{c}^{(i)}, \boldsymbol{\kappa}, \boldsymbol{\xi})$ , which is the product of all individual likelihoods. In fact, when the number of individuals  $M$  grows, the automatic differentiation tool needed to perform HMC will have to take care of differentiating with respect to the full likelihood, which is going to be a very long expression, where the many algebraic operations for its computation involve large matrices such as  $\tilde{\mathbf{A}}_k$ ,  $\tilde{\boldsymbol{\Sigma}}_k$  etc. Evaluating the gradient of such a large expression at every proposed parameter, will cause a considerable computational overhead. Of course, the complexity would be greatly reduced if the inference was based on data-summarization  $S(\mathbf{y})$  rather than  $\mathbf{y}$ , see the end of Section 2, since the dimensions of eg.  $\tilde{\mathbf{A}}_k$  and  $\tilde{\boldsymbol{\Sigma}}_k$  depend on the dimensions of  $\mathbf{y}$ . Secondly, when using HMC to propose fixed-effects  $\boldsymbol{\kappa}$  and  $\boldsymbol{\xi}$  in (24), it is not

possible to utilize one of the main benefits of our methodology, which is the self-tuning proposal sampler (and surrogate posterior)  $q_{\boldsymbol{\phi}}$ , that has desirable abilities to explore multimodal surfaces (Häggström et al. 2024). On the other hand, when considering all parameters to be individual as in (26)-(27), the proposal sampler  $q_{\boldsymbol{\phi}}$  can be used to propose all the  $\mathbf{c}^{(i)}$  (which include  $(\boldsymbol{\kappa}^{(i)}, \boldsymbol{\xi}^{(i)})$ ).

## 6.2 On the reduction of $K$ and of the sizes of $\tilde{\boldsymbol{\phi}}$ and $\boldsymbol{\phi}$

We have previously mentioned that our SeMPLE methodology incorporates ways to reduce the number of mixture components  $K$  automatically and hence the size of  $\tilde{\boldsymbol{\phi}}$  (this implies that the size of  $\boldsymbol{\phi}$  is also reduced since the latter is algebraically obtained from  $\tilde{\boldsymbol{\phi}}$ ). The dimension  $D(\tilde{\boldsymbol{\phi}})$  of  $\tilde{\boldsymbol{\phi}}$  is given by  $D(\tilde{\boldsymbol{\phi}}) = (K - 1) + K(d_{on}(q + p + s) + d_{on} + (q + p + s) + \text{nbpar}_{\Sigma} + \text{nbpar}_{\Gamma})$ , see Appendix B for details, and what we want to consider in this section is that by reducing  $K$  in a dynamic fashion, while SeMPLE runs from round  $r$  to round  $r + 1$ , the value of  $D(\tilde{\boldsymbol{\phi}})$  is drastically reduced, which is beneficial as the EM algorithm will have to explore a lower-dimensional surface. See Table 1, reporting the values of  $D(\tilde{\boldsymbol{\phi}})$  for the three applications we considered. The starting value of  $K$  (round  $r = 0$ ) is determined via BIC, as illustrated in Appendix B, and is then reduced by eliminating, in each round, those components  $k$  having coefficients  $\tilde{\eta}_k$  smaller than some positive threshold. The specific thresholds are specified in the results sections. Moreover, as mentioned in Section 2, in our case-studies we did not summarize the data  $\mathbf{y}$  via some informative summary function  $S(\cdot)$ , but if we did, the number of parameters  $D(\tilde{\boldsymbol{\phi}})$  would be greatly reduced, as in such case the term  $d_{on}$  would be much smaller ( $d_{on}$  would equal the size of  $S(\mathbf{y})$  for a vector of summaries induced by  $S(\cdot)$ ).

## 7 Examples on simulated and real biological data

We evaluate the performance of SeMPLE for mixed-effects models through three case studies. First, we examine a state-space SDEM with latent dynamics driven by Ornstein-Uhlenbeck SDEs. This example is particularly relevant as exact Bayesian inference is feasible without relying

**Table 1:** The number of mixture components  $K$  and the number  $D(\tilde{\phi})$  of mixture-model parameters  $\tilde{\phi}$  for each round  $r$  of SeMPLE.

Ornstein-Uhlenbeck			
round ( $r$ )	0	1	2
$K$	10	8	4
$D(\tilde{\phi})$	15,959	12,767	6,383
mRNA simulated data			
round ( $r$ )	0	1	2
$K$	10	9	5
$D(\tilde{\phi})$	24,149	21,734	12,074
mRNA real data			
round ( $r$ )	0	1	2
$K$	5	5	3
$D(\tilde{\phi})$	89,774	89,774	53,864

on pseudomarginal methods, providing a "gold-standard" reference posterior for comparison with SeMPLE inference. Next, we present two case studies where the reference posterior is obtained using a pseudomarginal (particle MCMC) sampler. These examples utilize the SDE model from Pieschner et al. (2022), which describes translation kinetics following mRNA transfection. The first case involves a simulation study, followed by an analysis with real data from Fröhlich et al. (2018). The model is two-dimensional, with only one observed component, and SeMPLE inference is compared to exact pseudomarginal inference obtained using the PEPsDI framework (Persson et al. (2022)).

## 7.1 Ornstein-Uhlenbeck state-space model

The Ornstein-Uhlenbeck process is defined by the following SDE,

$$dX_t^{(i)} = c_1^{(i)}(c_2^{(i)} - X_t^{(i)})dt + c_3^{(i)}dW_t^{(i)}, \quad (28)$$

where the  $\{W_t^{(i)}\}_{t \geq 0}$  are independent Wiener processes. In this example,  $\{X_t^{(i)}\}_{t \geq 0}$  is one-dimensional. We consider the following state-space

model, for  $i = 1, \dots, M$ :

$$\begin{cases} dX_t^{(i)} = c_1^{(i)}(c_2^{(i)} - X_t^{(i)})dt + c_3^{(i)}dW_t^{(i)} \\ Y_t^{(i)} = X_t^{(i)} + \epsilon_t^{(i)}, \quad \epsilon_t^{(i)} \sim \mathcal{N}(0, \xi^2), \end{cases} \quad (29)$$

where  $\{Y_t\}_{t \geq 0}$  is the observed process. The transition densities for the latent dynamics are known, and hence the Euler-Maruyama discretization is not needed to simulate the SDE (28) numerically. Instead we use the following exact simulation scheme, which is induced by the exact transition density

$$X_{t+\Delta_t}^{(i)} = c_2^{(i)} + (X_t^{(i)} - c_2^{(i)})e^{-c_1^{(i)}\Delta_t} \times \sqrt{\frac{c_3^{(i)}}{2c_1^{(i)}}(1 - e^{-2c_1^{(i)}\Delta_t})} \times u_t^{(i)}, \quad (30)$$

where  $u_t^{(i)} \stackrel{\text{iid}}{\sim} \mathcal{N}(0, 1)$ .

### 7.1.1 Inference setup

We consider an inference setting similar to the one in Wiquist et al. (2021) and Persson et al. (2022). Data were simulated for  $M = 40$  individuals at 50 equidistant time points from  $t = 0.2$  to  $t = 10$  ( $\Delta_t = 0.2$ ), and with initial value  $X_0 = 0$  at  $t = 0$ . We set a Gaussian population distribution  $\log(c_1^{(i)}, c_2^{(i)}, c_3^{(i)}) \sim \mathcal{N}(\mu, \tau^{-1})$ , where the true data generating values for the population parameters were set to  $\mu = (-0.7, 2.3, -0.9)$  and  $\tau = (4, 10, 4)$ . Similarly to Wiquist et al. (2021), the prior of  $\eta = (\mu_1, \mu_2, \mu_3, \tau_1, \tau_2, \tau_3)$  was set to be  $\pi(\eta) = \prod_{j=1}^3 \pi(\mu_j | \tau_j) \pi(\tau_j)$ , where the  $\pi(\mu_j | \tau_j)$  and the  $\pi(\tau_j)$  are in equation (31):

$$\begin{cases} \mu_j | \tau_j \sim \mathcal{N}(\mu_{0j}, (\lambda_j \tau_j)^{-1}), & j = 1, 2, 3, \\ \tau_j \sim Ga(\alpha_j, \beta_j). \end{cases} \quad (31)$$

The prior parameter values can be found in Supplementary Material. The "Normal-Gamma" prior (31) allows us to benefit from conjugacy when sampling  $\eta$  directly from a Normal-Gamma distribution in the third Gibbs sampler step. The prior of  $\tau$  is shifted a bit from the setup in Wiquist et al. (2021), to avoid having small precisions resulting in a large variance in  $\mu$ , and



consequentially unreasonable prior-predictive simulated data. The data-generating value of the noise parameter is  $\log(\xi) = -1.2$ , and we used as prior  $\log(\xi) \sim \mathcal{N}(0, 1)$ .

### 7.1.2 Settings for SeMPLE

We first determined an appropriate number of mixture components  $K$ , using the BIC criterion (Appendix B), see Figure B1. Consequently, we set the starting number of components to be  $K = 10$ , which is a number that is allowed to decrease between the SeMPLE rounds, as discussed in Section 6. In this case, the threshold for removing mixture components having small mixture probabilities was set to 0.005 (ie in each round of SeMPLE, any component  $k$  having  $\hat{\eta}_k < 0.005$  is removed). The covariance matrices  $\Sigma_k$  and  $\tilde{\Sigma}_k$  in the GLLiM models were set to be unconstrained, i.e. fully parameterized. The number of prior predictive samples is  $N = 10,000$  and the number of surrogate posterior samples per individual is  $N_s = 1,000$ .

### 7.1.3 Results

The prior and marginal posteriors for the “common parameters” (i.e. shared between subjects)  $\eta$  and  $\xi$  (Figure 2) are obtained using both SeMPLE and exact Bayesian inference (MCMC). Exact inference is obtained using the three steps of the Gibbs sampler, where the exact likelihood provided by the Kalman filter is used in the Metropolis-within-Gibbs steps (7)-(8). Therefore, exact inference is used as a reference to assess the accuracy of the SeMPLE approach in Algorithm 1. For exact inference, 200k posterior samples were produced in total, where the first 100k were discarded as burn-in samples, and the remaining 100k samples were thinned (every tenth sample was retained) to obtain the final 10k samples, which is the same size produced with SeMPLE. The inference obtained with SeMPLE is very satisfying in the sense that it is similar to exact inference (Figure 2). Not much is learned about the population precisions  $\tau$ , but this is most likely due to the low number of individuals  $M = 40$  as results are the same with the exact likelihood. We notice a slightly higher variance in the SeMPLE posterior of  $\mu_{c_3}$  and  $\log \xi$  compared to exact inference. The traceplots in Supplementary sections show that

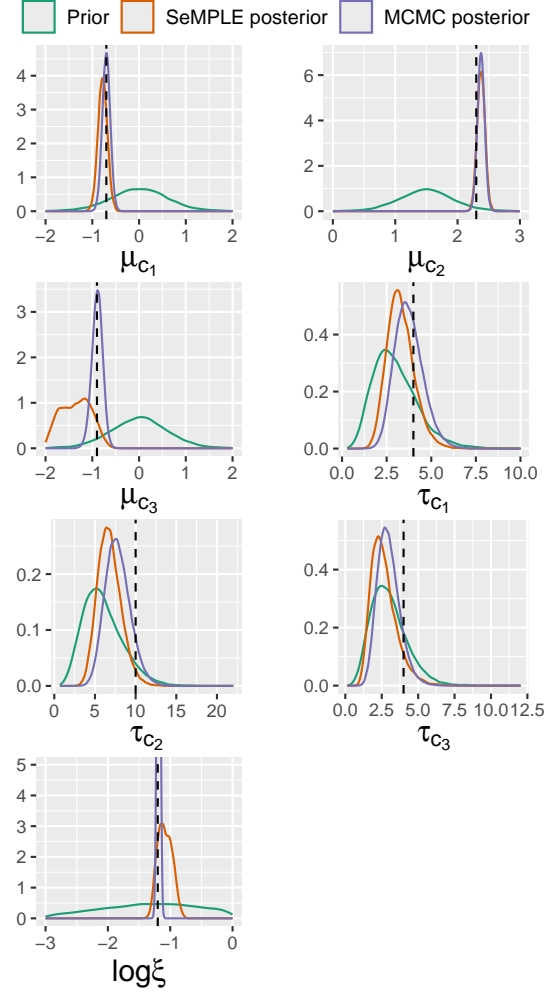


**Fig. 2:** Ornstein-Uhlenbeck: marginal posteriors from 10k posterior samples from MCMC using the exact likelihood (purple) and SeMPLE (orange). Priors are in green. The dashed lines are the true parameter values.

for MCMC iterations when  $\mu_{c_3}$  is slightly overestimated,  $\log \xi$  is slightly underestimated, and the other way around. However, posterior predictive checks (Figure 3) support that the overall uncertainty about the observed dynamics is well captured. Extra results, such as traceplots of the SeMPLE posterior samples (Supplementary Material section S3.1), show the excellent mixing of the chains obtained with SeMPLE. Moreover, inference for the individual (subject specific) parameters  $c^{(i)}$ , remarkably captures the true values of the data-generating  $c^{(i)}$ 's (Supplementary

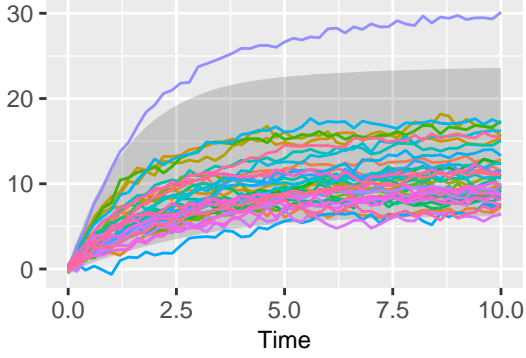


**Fig. 3:** Ornstein-Uhlenbeck: Posterior-predictive simulations from SeMPLE and data (colored lines, 40 individuals). In grey is the area between the 2.5th and 97.5th percentile from 10k posterior-predictive simulations obtained from SeMPLE.

Material section S3.1). This is the case for our experiment involving  $M = 40$  individuals, and we have no reason to suspect that an opposite result would be achieved for a larger  $M$ . We note that the number of mixture components is reduced from  $K = 10$  to  $K = 4$  after the second training of the GLLiM model, resulting in a substantially lower total number of parameters for the surrogate likelihood (Table 1).

## 7.2 mRNA transfection model

We consider the SDE model in a simulation study originally used to describe translation kinetics following mRNA transfection (Pieschner et al. (2022)). The dataset consists of time-lapse microscopy images capturing the fluorescence intensity of cells over at least 30 hours, with measurements taken every 10 minutes (Fröhlich et al. (2018)). During the first hour, cells were incubated with mRNA lipoplexes before being washed to prevent further uptake. As the released mRNA is translated into a green fluorescent protein (GFP), the cell fluorescence is tracked over time. The SDE below is used to study the translation kinetics of one cell, based on the observed fluorescence trajectory of individual cells after transfection with mRNA encoding for GFP, where the two-dimensional stochastic process  $(m(t), p(t))$  where  $m(t)$  represents the amount of mRNA molecules at time  $t$ , and  $p(t)$  is the amount of GFP molecules

at time  $t$ . The SDEM is given by

$$d \begin{pmatrix} m^{(i)} \\ p^{(i)} \end{pmatrix} (t) = \begin{pmatrix} -\delta^{(i)} \cdot m^{(i)}(t) \\ k^{(i)} \cdot m^{(i)}(t) - \gamma^{(i)} \cdot p^{(i)}(t) \end{pmatrix} dt + \begin{pmatrix} \sqrt{\delta^{(i)} \cdot m^{(i)}(t)} & 0 \\ 0 & \sqrt{k^{(i)} \cdot m^{(i)}(t) + \gamma^{(i)} \cdot p^{(i)}(t)} \end{pmatrix} dB_t^{(i)} \quad (32)$$

$$(\delta^{(i)}, \gamma^{(i)}, k^{(i)}) \sim \pi(\delta, \gamma, k | \boldsymbol{\eta}), \quad i = 1, \dots, M,$$

where the  $B_t^{(i)}$  are two-dimensional standard Brownian motions. It is assumed that all mRNA molecules (within one cell) are released at once from the lipoplexes and denote this initial time point by  $t_0$ . Before  $t_0$ , there are neither mRNA nor GFP molecules, and at  $t_0$ , an amount  $m_0$  of mRNA molecules is released, i.e

$$\begin{pmatrix} m^{(i)}(t) \\ p^{(i)}(t) \end{pmatrix} = \begin{pmatrix} 0 \\ 0 \end{pmatrix} \quad \text{for } t < t_0$$

while  $m^{(i)}(t_0) = m_0$  and  $p^{(i)}(0) = 0$ . We take as observable mapping

$$y^{(i)}(t_j) = \log(\text{scale} \cdot p^{(i)}(t_j) + \text{offset}) + \varepsilon^{(i)}(t_j), \quad (33)$$

where  $\varepsilon^{(i)}(t_j)$  is iid Gaussian measurement error  $\varepsilon^{(i)}(t_j) \sim \mathcal{N}(0, \sigma^2)$ ,  $j = 1, \dots, n$ , and  $t_1, \dots, t_n$  are observational time instants (see further below). Note that the observations depend only indirectly on process  $\{m^{(i)}(t)\}$ , and only  $\{p^{(i)}(t)\}$  is observed. The model parameters  $(\delta, \gamma, k)$  are treated as parameters that vary between individuals, i.e.  $\boldsymbol{c}^{(i)} = (\delta^{(i)}, \gamma^{(i)}, k^{(i)})$ . The remaining model parameters  $(m_0, \text{scale}, \text{offset}, \sigma)$  are treated as parameters that do not vary between individuals, where  $\boldsymbol{\kappa} = (m_0, \text{scale}, \text{offset})$  and  $\boldsymbol{\xi} = \sigma$ . The choice of individual parameters and individual-constant parameters is similar to Arruda et al. (2024). In Section 7.2.8 we also consider different assumptions where all parameters are set to be random effects, and discuss implications in terms of scalability.

### 7.2.1 Inference setup for simulated data

In this example, we fix  $t_0 = 0$  and do not infer it. This choice enables a direct comparison with the pseudomarginal (particle MCMC) inference produced by the PEPSDI framework (Persson et al.

2022), which does not currently support inference of the initial simulation time  $t_0$ . However, in the real-data case-study that follows in next sections we infer also  $t_0$  (only with SeMPLE). Inference is performed on the log-scale and the population distribution is assumed to be Gaussian,  $\log(\mathbf{c}^{(i)}) \sim \mathcal{N}(\boldsymbol{\mu}, \boldsymbol{\tau}^{-1})$ , where the true values of the population distribution parameters used to generate the simulated data was set to  $\boldsymbol{\mu} = (-0.694, -3, 0.027)$  and  $\boldsymbol{\tau} = (10, 10, 10)$ . It has been shown that SDE modelling improves identifiability of parameters, compared to using a corresponding ODE model (Pieschner et al. 2022). Nevertheless, some parameters are still unidentifiable (for details see in particular supplementary section A.4.1 in Pieschner et al. 2022).

Here the exact transition densities are unavailable, and solutions to the SDE (32) are simulated using an Euler-Maruyama scheme implemented in Rcpp (Eddelbuettel et al. 2024) from  $t = t_0$  to  $t = 30$ , with step size 0.01. The observed time series is interpolated from the Euler-Maruyama approximation at  $n = 60$  equidistant time points from  $t_1 = 0.5$  to  $t_n = 30$ . We simulate  $M = 40$  individuals according to this setup. The prior distributions are set to be Normal-Gamma for the random effects and Gaussian on the log-scale for the fixed effects. Prior parameters can be found in Supplementary Material section S3.2.

### 7.2.2 Settings for SeMPLE

The starting number of mixture components for the mixture models was set to  $K = 10$ , according to the Bayesian information criterion (Figure B1), with covariance matrices for the mixture components specified to be full and unconstrained. The threshold to remove mixture components with small mixture probabilities was set to 0.005. The number of prior-predictive samples is  $N = 50,000$ , and the number of surrogate posterior samples per individual is  $N_s = 1000$ . Additionally, the number of burn-in samples when sampling the individual parameters was set to  $N_{MH} = 10$ , to improve the mixing of the individual parameter Markov chains.

### 7.2.3 Setup for the pseudomarginal method PEPSDI

To assess the quality of the approximate inference obtained by SeMPLE, we run PEPSDI with the inference setup described in section 7.2.1. To

avoid typical initialization problems with possibly high-rejection rates caused by setting starting parameters far from the bulk of the posterior, we initialize PEPSDI at the same (true) parameter values used to generate the observed data. We produce 50k posterior samples with PEPSDI, which are then thinned by retaining every fifth draw, to obtain 10k posterior samples that are used to report inference (this is the same number of posterior samples produced with SeMPLE). The number of particles was manually set to 150 for every individual, and the initialization of the proposal covariance matrix for the fixed-effects ( $\boldsymbol{\kappa}, \boldsymbol{\xi}$ ) was tuned manually to improve the mixing of the Markov chains of these parameters.

### 7.2.4 Results from simulated data

The posterior distributions of the population means  $\boldsymbol{\mu}$  and population precisions  $\boldsymbol{\tau}$  returned by SeMPLE are virtually identical to exact (pseudo-marginal) inference returned by PEPSDI (Figure 4). The same applies to the measurement error's standard deviation  $\sigma$  and the offset parameter. The posterior plots indicate that the  $m_0$  and scale parameters are more challenging to infer. This difficulty is also evident in the corresponding posterior plots in Arruda et al. (2024). In addition to the posterior density plots, posterior predictive checks for several exemplary individuals are given in Supplementary Material. The SeMPLE runtime throughout the  $R$  rounds, was 346 minutes  $\approx 5.8$  hours. In addition to this, the determination of the initial  $K$  via the BIC took 13 minutes. The PEPSDI runtime to produce the same number of posterior samples (10k) was approximately 29.8 hours, using the artificially favorable setup where we avoided investing time in the search for a suitable starting value for the parameters. SeMPLE was run on a laptop with an 8-core Intel Core i5-10310U CPU and 16GB of RAM. We emphasize that a much faster version is in Section 7.2.8, corresponding to the two-steps Gibbs described in Section 6.1.

### 7.2.5 Inference setup with real data

We now use the same SDEMEM as in the simulated data example to test our method on the real-world dataset from Fröhlich et al. (2018), to which we refer the reader for details regarding the experimental procedures. This data was also been

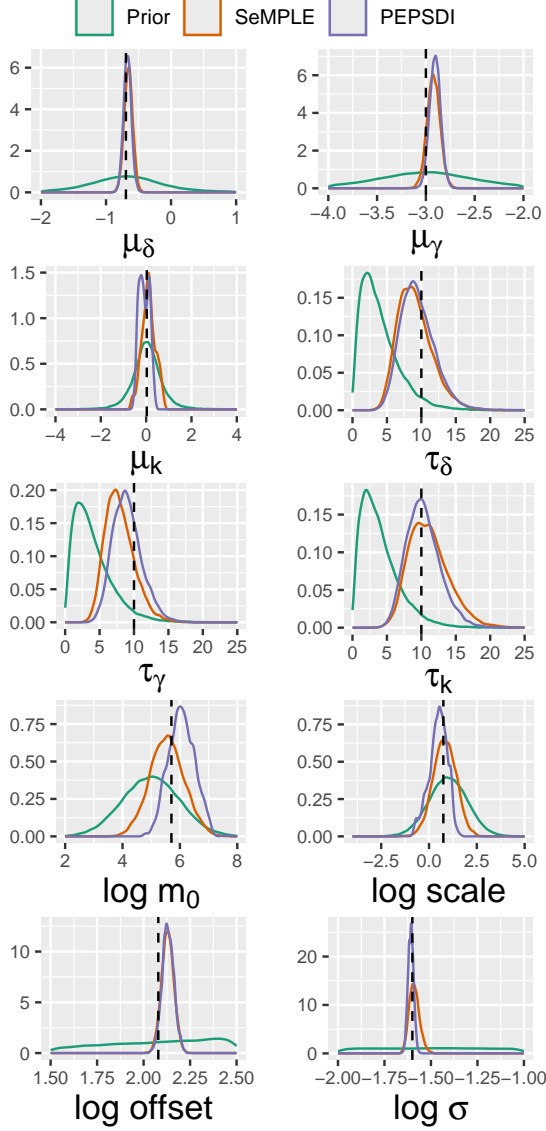


**Fig. 4:** mRNA model with 40 simulated individuals: marginal posteriors obtained with SeMPLE (orange) and with PEPSDI (purple). Priors are in green. The dashed lines are the true parameter values that were used to generate the observed data.

analysed in Pieschner et al. (2022), where the initial ODE model was extended to an SDE model with improved parameter identifiability, however no new methodology was presented. We extend their work by providing a new methodology that can be applied to the SDE formulation of the model with satisfying results. We consider the first  $M = 40$  individuals from the data set labeled

“20164027\_mean\_eGFP” in Fröhlich et al. (2018). The raw data is then log-transformed in accordance with the observable mapping (33). Note that the real data set has 180 measurements for each individual, as opposed to the 60 measurements in the simulated data setup described in 7.2.1. To allow more flexibility, the prior distribution of the population parameters are set to be independent Gaussian for the mean  $\mu$  and Gamma-distributed precision  $\tau$  instead of a prior Normal-Gamma distribution. The prior parameters can be found in Supplementary Material section S4. Consequentially, it is no longer possible to sample the population parameters  $\eta$  directly, since we cannot exploit conjugacy here. Instead, we use HMC to sample the population parameters efficiently in the Gibbs sampler. Note that, as opposed to the setup with simulated data, we now infer the initial time point  $t_0$  as a parameter that varies between individuals, i.e.  $c^{(i)} = (\delta^{(i)}, \gamma^{(i)}, k^{(i)}, t_0^{(i)})$ ; however we can only do so via SeMPLE, as PEPSDI currently does not allow to infer the starting time  $t_0$ , and therefore we cannot compare the SeMPLE results with exact Bayesian (pseudomarginal) inference. This is not a problem per-se, as we have already shown such a comparison and the SeMPLE reliability in the simulation study.

### 7.2.6 Settings for SeMPLE with real data

Similarly to the setting with simulated data in section 7.2.2 we set the GLLiM covariance matrices for the mixture components to be full and unconstrained. The number of mixture components was set to  $K = 5$  according to the BIC (Figure B1). Note that the number of prior-predictive samples was reduced from 50k with the simulated data to 10k for the real data setting with 180 observations per time series. This was initially done to reduce the computational effort, but it was found that this reduction in prior-predictive samples did not have a negative impact on the quality of the inference.

### 7.2.7 Results from real data example

The model parameter  $t_0$  can easily be identified with our methodology, as demonstrated by the posterior mean  $\mu_{t_0}$  and precision  $\tau_{t_0}$  (Figure 5). In

addition to this, we note that the posterior modes of several parameters (e.g.  $\mu_\delta$ ,  $\log \sigma$ ,  $\log \text{offset}$ ) lie in the tails of their prior distributions, suggesting that we are not heavily reliant on an informative prior specification (Figure 5). To validate the quality of the inference, we provide posterior predictive simulations for all individuals (Figure 6). It is clear that the uncertainty about the observed dynamics is well captured and that our posterior inference is consistent with the observed data. Traceplots and additional individual posterior predictive simulation plots can be found in the Supplementary Material section S4.

The SeMPLE runtime was 176 minutes  $\approx$  2.9 hours. In addition to this, the runtime to determine the initial  $K$  via the BIC for this setup was 10 minutes. Note that the number of posterior samples was reduced, compared to the simulated data setup, to reduce the runtime.

### 7.2.8 Scalable approach using exclusively random-effects

As explained in Section 6.1, a major computational bottleneck in the framework presented so far is the second step of the Gibbs sampler (24), where the full likelihood (the product of all individual likelihoods) is used within HMC. Here we consider inference with the two-steps “reduced” Gibbs sampler from Section 6.1. The population distribution for the translation kinetics model after mRNA transfection can then be rewritten as

$$\log(\delta^{(i)}, \gamma^{(i)}, k^{(i)}, t_0^{(i)}, m_0^{(i)}, \text{scale}^{(i)}, \text{offset}^{(i)}, \sigma^{(i)}) \sim \mathcal{N}(\boldsymbol{\mu}, \boldsymbol{\tau}^{-1}), \quad i = 1, \dots, M. \quad (34)$$

Therefore, compared to previous analyses, here  $(m_0^{(i)}, \text{scale}^{(i)}, \text{offset}^{(i)}, \sigma^{(i)})$  are also random effects. We run SeMPLE with the same  $M = 40$  individuals from the real data set as in Section 7.2.7. The runtime to produce 1,000 posterior samples is 37 minutes (Figure S11), a significant reduction compared to the corresponding runtime with fixed-effects of 2.9 hours in section 7.2.7. The population posterior distributions are similar to the results when the model parameters  $m_0, \text{scale}, \text{offset}$  and  $\sigma$  are treated as constant parameters shared by all individuals (Figure 5). Interestingly, we do not learn much about the parameters  $m_0$  and  $\text{scale}$  (Figure 5), since the posteriors do not differ significantly from the

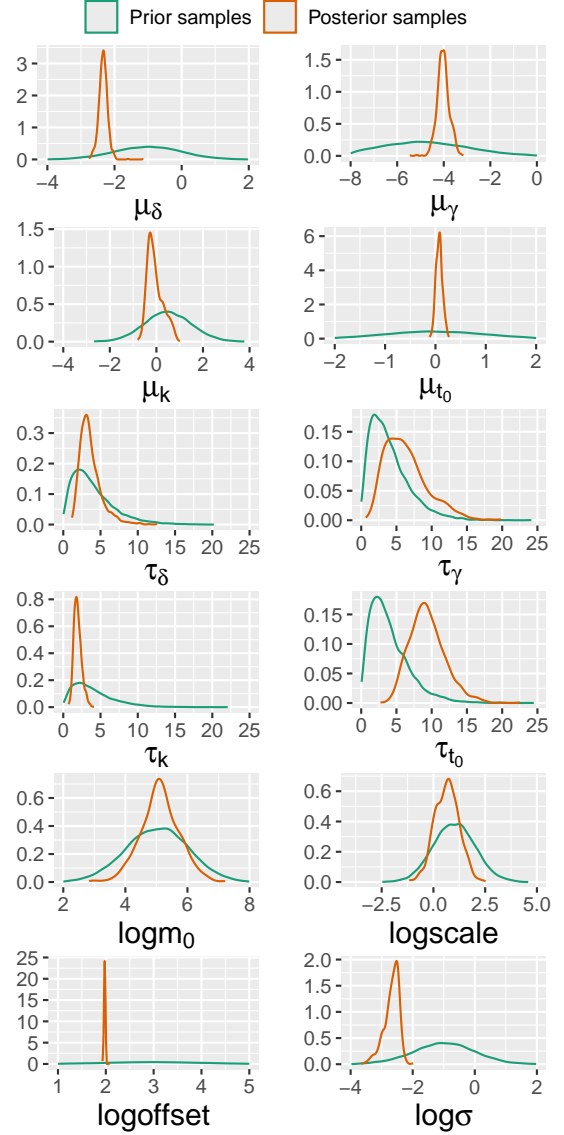


**Fig. 5:** mRNA model with real data (40 individuals): marginal posteriors (1,000 samples) obtained with SeMPLE (orange) and priors (green). Parameters  $m_0, \text{scale}, \text{offset}$  and  $\sigma$  are treated as fixed effects.

priors, but when treating these parameters as random-effects (Figure S11) we are able to learn more about the population mean of  $m_0$  and  $\text{scale}$ . We note that for many of the population precisions  $\boldsymbol{\tau}$ , the posterior distributions are similar to the priors, except for the population precisions  $\tau_{t_0}$  and  $\tau_{\text{offset}}$ . This suggests that a data set of



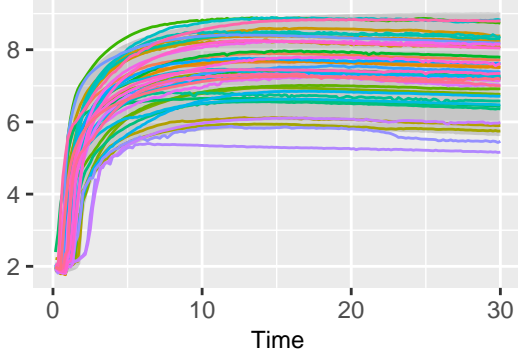


**Fig. 6:** mRNA model with real data: posterior-predictive simulations for 40 individuals using SeMPLE (colored lines are observed data). In grey is the area between the 2.5th and 97.5th percentile from 1k posterior-predictive simulations obtained from SeMPLE.

40 individuals is not large enough to infer the population variance of all the model parameters.

### 7.2.9 Runtime scaling

To further investigate how the runtime of the SeMPLE algorithm scales with the number of individuals  $M$ , we perform a simulation study for increasing  $M$ . We report the run times both with the most general SeMPLE algorithm for the three-steps Gibbs approach (with setup described in Section 7.2.5), and the corresponding setup with the scalable approach described in Section 7.2.8. However, to ease the calculations, here we use simulated data with 60 observations for each individual. The number of prior predictive samples  $N = 10,000$  and the number of surrogate posterior samples per individual  $N_s$  is adjusted according to  $MN_s = 40,000$ , to have a fixed size of the data set  $\mathcal{D}_1$  that the updated surrogate models are trained on. The number of Gaussian mixture components was set to  $K = 10$  for both algorithm versions to make comparisons fair, even though previous BIC results (Figure B1) suggests a smaller  $K$  could be used. The number of burnin samples is set to  $N_{MH} = 10$  in all simulations. We measure the wall-clock runtime to obtain 1,000 posterior samples from the corresponding Gibbs sampler, this includes the training of the surrogate likelihood both on prior-predictive data and on samples from the surrogate posterior (Figure 7). Here, the

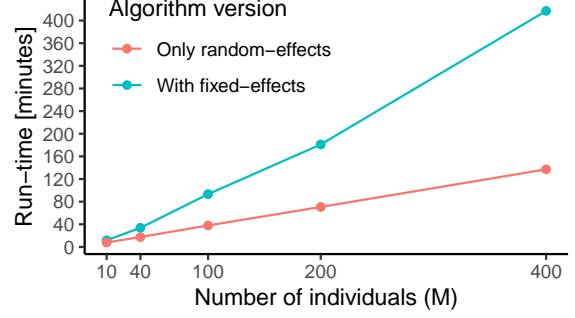


**Fig. 7:** SeMPLE runtime to obtain 1,000 posterior samples as a function of the number of individuals. The blue line corresponds to the algorithm version that also include constant parameters (fixed-effects) and the red line to the version with only individual parameters (random-effects).

“scalable approach” two-steps Gibbs is denoted with “only random-effects”, and the three-steps Gibbs with “with fixed-effects”. For the scalable approach the runtime clearly scales linearly with the number of individuals. This is to be expected since the sampling via Gibbs (i.e. excluding the mixtures fitting) typically makes up the majority of the runtime, and this scales linearly with  $M$  when no parallelization is performed. The runtime of fitting the surrogate models is typically negligible in comparison to the Gibbs sampling, especially when the size of the second training data set  $MN_s$  is kept constant for varying  $M$ .

Connecting to the conjecture that the number of individuals ( $M = 40$ ) in the data set was not large enough to infer the population precision (Figure S11), we refer to a simulation study in Supplementary Material using  $M = 200$  (Figure S7). We note that as opposed to the result where the posterior population precisions distributions are virtually identical with their respective prior distributions (Figure S11), now, the posterior distributions of the population precisions are clearly different from their prior distributions (Figure S7), suggesting that we learn about the population precisions from the data, which are centered around the true data generating value.

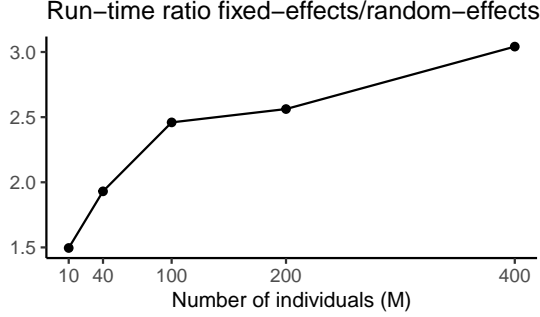


**Fig. 8:** Ratio of SeMPLE runtimes for a model that include fixed-effects and the one having only random-effects, corresponding to the data in Figure 7.

## 8 Discussion and conclusion

This study introduces a novel simulation-based (Bayesian) inference method for stochastic non-linear mixed-effects models. More specifically, we focused on mixed-effects driven by SDEs (SDEMEMs). The method addresses the challenge of providing general and still computationally efficient methodology in this setting. Our SeMPLE methodology builds amortized approximations of the intractable likelihood and of the posterior using mixtures of experts, and then proceeds at refining such approximations for given observed data, without using neural conditional estimation, unlike in state-of-the-art SBI methodology. For the several case studies we considered, including a SDEMEM for translation kinetics model after mRNA transfection, we compared our inference against gold-standard Bayesian inference, either using exact or asymptotically exact (pseudo-marginal) MCMC samplers (Wqvist et al. 2021; Persson et al. 2022). In all cases we show that with SeMPLE we obtain inference that is very similar to exact Bayes, but with the additional advantage of allowing inference for a much larger number of individuals than could be possible with particle-based MCMC approaches, as further discussed below. In terms of generality, SeMPLE provides full Bayesian inference with the option of treating any model parameter as either a fixed or a random effect, unlike methods where fixed effects are artificially modelled as random effects with a small fixed variance (Arruda et al. (2024)). In addition, SeMPLE allows to infer the time point  $t_0$  of the

discrete jump in the SDE solution as a model parameter, instead of being forced to assume  $t_0$  as known, a limitation present in both Pieschner et al. (2022) and Persson et al. (2022).

We have explored the scalability of our methodology with respect to an increasing number of individuals  $M$  (Section 7.2.9), and we have provided an additional (and slightly less general) version of our method that has an improved scalability (Section 7.2.8). We have shown that, with the more scalable version of SeMPLE, we can fit SDEMEMs to several hundreds of individuals using a standard laptop, which is particularly notable, and would not have been possible with the particle MCMC (pMCMC) approaches in, e.g., Persson et al. (2022), without considerable tuning (e.g. tuning for the number of particles, the usage of “guided” paths-solutions for the particle filters). Moreover, pMCMC is not an amortized approach and requires reruns for every new considered dataset. Still, for SeMPLE there is room for improvement in terms of the scalability in the number of individuals  $M$ . For example, full Bayesian inference for SDEMEMs with several thousands of individuals, can be computationally demanding for SeMPLE when running on a standard laptop, but could of course be accommodated on a computer cluster. We note that the Gibbs sampler step with the individual parameters in (23) allows for parallelization, and with a large number of individuals this could reduce the runtime significantly. Another methodology, which targets scalability but using amortized neural density estimators, is in Arruda et al. (2024). However, in Arruda et al. (2024) the focus is not on fully Bayesian inference (even though the neural density estimator can be used in this regard), but instead on maximum likelihood estimation and uncertainty quantification through profile likelihood analysis. As mentioned previously, another limitation in Arruda et al. (2024) is that of not modelling fixed effects in full generality. It is difficult to construct inference methods for SDEMEMs that are computationally efficient without making simplifications at the cost of generality. In this regard, we identify a need for further research in this field while providing a significant contribution in this direction.

## Acknowledgments

HH, UP and MC acknowledge support from the Swedish Research Council (Vetenskapsrådet 2019-03924 and 2023-04319). SP and MC acknowledge support from the Swedish Foundation for Strategic Research (FFL15-0238). UP acknowledges support from the Chalmers AI Research Centre (CHAIR). The computations were enabled by resources provided by the National Academic Infrastructure for Supercomputing in Sweden (NAISS), partially funded by the Swedish Research Council through grant agreement no. 2022-06725.

## Statements and declarations

### Competing interests

The authors declare no competing interests.

## References

- Andrieu, C., Doucet, A., Holenstein, R.: Particle Markov chain Monte Carlo methods. *Journal of the Royal Statistical Society Series B: Statistical Methodology* **72**(3), 269–342 (2010)
- Andrieu, C., Roberts, G.O.: The pseudo-marginal approach for efficient Monte Carlo computations. *The Annals of Statistics* (2009)
- Arruda, J., Schälte, Y., Peiter, C., Teplytska, O., Jaehde, U., Hasenauer, J.: An amortized approach to non-linear mixed-effects modeling based on neural posterior estimation. In: *Proceedings of the 41st International Conference on Machine Learning*, vol. 235, pp. 1865–1901 (2024)
- Åkesson, M., Singh, P., Wrede, F., Hellander, A.: Convolutional neural networks as summary statistics for approximate Bayesian computation. *IEEE/ACM Transactions on Computational Biology and Bioinformatics* **19**(6), 3353–3365 (2021)
- Botha, I., Kohn, R., Drovandi, C.: Particle methods for stochastic differential equation mixed effects models. *Bayesian Analysis* **16**(2), 575–609 (2021)
- Buckwar, E., Tamborrino, M., Tubikanec, I.: Spectral density-based and measure-preserving ABC for partially observed diffusion processes. an illustration on hamiltonian SDEs. *Statistics and Computing* **30**(3), 627–648 (2020)
- Cranmer, K., Brehmer, J., Louppe, G.: The frontier of simulation-based inference. *Proceedings of the National Academy of Sciences* **117**(48), 30055–30062 (2020)
- Craigmile, P., Herbei, R., Liu, G., Schneider, G.: Statistical inference for stochastic differential equations. *Wiley Interdisciplinary Reviews: Computational Statistics* **15**(2), 1585 (2023)
- Chen, Y., Zhang, D., Gutmann, M.U., Courville, A., Zhu, Z.: Neural approximate sufficient statistics for implicit models. In: *International Conference on Learning Representations* (2021)
- Deleforge, A., Forbes, F., Horaud, R.: High-dimensional regression with Gaussian mixtures and partially-latent response variables. *Statistics and Computing* **25**(5), 893–911 (2014)
- Davidian, M., Giltinan, D.M.: Nonlinear models for repeated measurement data: an overview and update. *Journal of agricultural, biological, and environmental statistics* **8**, 387–419 (2003)
- Diggle, P.J., Heagerty, P., Liang, K.-Y., Zeger, S.: *Analysis of Longitudinal Data*. Oxford University Press, ??? (2002)
- Delaunoy, A., Hermans, J., Rozet, F., Wehenkel, A., Louppe, G.: Towards reliable simulation-based inference with balanced neural ratio estimation. *Advances in Neural Information Processing Systems* **35**, 20025–20037 (2022)
- Del Moral, P., Murray, L.M.: Sequential Monte Carlo with highly informative observations. *SIAM/ASA Journal on Uncertainty Quantification* **3**(1), 969–997 (2015)
- Durkan, C., Murray, I., Papamakarios, G.: On contrastive learning for likelihood-free inference. In: *International Conference on Machine Learning*, pp. 2771–2781 (2020). PMLR
- Eddelbuettel, D., Francois, R., Allaire, J., Ushey,

- K., Kou, Q., Russell, N., Ucar, I., Bates, D., Chambers, J.: Rcpp: Seamless R and C++ Integration. (2024). R package version 1.0.12. <https://CRAN.R-project.org/package=Rcpp>
- Fearnhead, P., Prangle, D.: Constructing summary statistics for approximate Bayesian computation: semi-automatic approximate Bayesian computation. *Journal of the Royal Statistical Society Series B: Statistical Methodology* **74**(3), 419–474 (2012)
- Fröhlich, F., Reiser, A., Fink, L., Woschée, D., Ligon, T., Theis, F.J., Rädler, J.O., Hasenauer, J.: Multi-experiment nonlinear mixed effect modeling of single-cell translation kinetics after transfection. *NPJ systems biology and applications* **4**(1), 42 (2018)
- Gillespie, D.T.: Exact stochastic simulation of coupled chemical reactions. *The journal of physical chemistry* **81**(25), 2340–2361 (1977)
- Gillespie, D.T.: The chemical langevin equation. *The Journal of Chemical Physics* **113**(1), 297–306 (2000)
- Gillespie, D.T.: Stochastic simulation of chemical kinetics. *Annu. Rev. Phys. Chem.* **58**(1), 35–55 (2007)
- Greenberg, D., Nonnenmacher, M., Macke, J.: Automatic posterior transformation for likelihood-free inference. In: *International Conference on Machine Learning*, pp. 2404–2414 (2019). PMLR
- Golightly, A., Wilkinson, D.J.: Bayesian parameter inference for stochastic biochemical network models using particle Markov chain Monte Carlo. *Interface focus* **1**(6), 807–820 (2011)
- Gabry, J., Češnovar, R., Johnson, A., Bronder, S.: Cmdstanr: R Interface to 'CmdStan'. (2024). R package version 0.8.1, <https://discourse.mc-stan.org>. <https://mc-stan.org/cmdstanr/>
- Higham, D., Kloeden, P.: *An Introduction to the Numerical Simulation of Stochastic Differential Equations*. SIAM, ??? (2021)
- Häggström, H., Rodrigues, P.L.C., Oudoumanesah, G., Forbes, F., Picchini, U.: Fast, accurate and lightweight sequential simulation-based inference using Gaussian locally linear mappings. *Transactions on Machine Learning Research* (2024). <https://openreview.net/forum?id=Q0nzpRcwWn>
- Lavielle, M.: *Mixed Effects Models for the Population Approach: Models, Tasks, Methods and Tools*. CRC press, ??? (2014)
- Miller, B.K., Cole, A., Forré, P., Louppe, G., Weniger, C.: Truncated marginal neural ratio estimation. *Advances in Neural Information Processing Systems* **34**, 129–143 (2021)
- Marin, J.-M., Pudlo, P., Robert, C.P., Ryder, R.J.: Approximate Bayesian computational methods. *Statistics and Computing* **22**(6), 1167–1180 (2012)
- Murphy, K.P.: Conjugate Bayesian analysis of the Gaussian distribution. <https://www.cs.ubc.ca/~murphyk/Papers/bayesGauss.pdf>. Accessed: 1 October 2024 (2007)
- Price, L.F., Drovandi, C.C., Lee, A., Nott, D.J.: Bayesian synthetic likelihood. *Journal of Computational and Graphical Statistics* **27**(1), 1–11 (2018)
- Perthame, E., Forbes, F., Deleforge, A., Devijver, E., Gallopin, M.: xLLiM: High Dimensional Locally-Linear Mapping. (2022). R package version 2.2.1
- Pieschner, S., Hasenauer, J., Fuchs, C.: Identifiability analysis for models of the translation kinetics after mRNA transfection. *Journal of Mathematical Biology* **84**(7), 56 (2022)
- Picchini, U.: Stochastic differential equations mixed-effects models. <https://umbertopicchini.github.io/sdemem/>. Accessed: 1 October 2024 (2024)
- Papamakarios, G., Murray, I.: Fast  $\epsilon$ -free inference of simulation models with Bayesian conditional density estimation. *Advances in Neural Information Processing Systems* **29** (2016)

- Papamakarios, G., Nalisnick, E., Rezende, D.J., Mohamed, S., Lakshminarayanan, B.: Normalizing flows for probabilistic modeling and inference. *The Journal of Machine Learning Research* **22**(1), 2617–2680 (2021)
- Pesonen, H., Simola, U., Köhn-Luque, A., Vuollekoski, H., Lai, X., Frigessi, A., Kaski, S., Frazier, D.T., Maneesoonthorn, W., Martin, G.M., Corander, J.: ABC of the future. *International Statistical Review* **91**(2), 243–268 (2023)
- Papamakarios, G., Sterratt, D., Murray, I.: Sequential Neural Likelihood: Fast Likelihood-free Inference with Autoregressive Flows. In: *Proceedings of the Twenty-Second International Conference on Artificial Intelligence and Statistics*, vol. 89, pp. 837–848. PMLR, ??? (2019)
- Persson, S., Welkenhuysen, N., Shashkova, S., Wqvist, S., Reith, P., Schmidt, G.W., Picchini, U., Cvijovic, M.: Scalable and flexible inference framework for stochastic dynamic single-cell models. *PLOS Computational Biology* **18**(5), 1–24 (2022)
- Robert, C., Casella, G.: *Monte Carlo Statistical Methods*. Springer (2004)
- Rezende, D., Mohamed, S.: Variational inference with normalizing flows. In: *International Conference on Machine Learning*, pp. 1530–1538 (2015). PMLR
- Radev, S.T., Schmitt, M., Pratz, V., Picchini, U., Koethe, U., Buerkner, P.: JANA: Jointly amortized neural approximation of complex Bayesian models. In: *Proceedings of the Thirty-Ninth Conference on Uncertainty in Artificial Intelligence*, pp. 1695–1706 (2023). PMLR
- Sisson, S.A., Fan, Y., Beaumont, M.: *Handbook of Approximate Bayesian Computation*. CRC Press, ??? (2018)
- Stan Development Team: *Stan Modeling Language Users Guide and Reference Manual*, version 2.32 (2023). <https://mc-stan.org/docs/2.32/reference-manual/index.html>
- Stan Development Team: *RStan: the R interface to Stan*. R package version 2.32.6 (2024). <https://mc-stan.org/>
- Schauer, M., Meulen, F., Zanten, H.: Guided proposals for simulating multi-dimensional diffusion bridges. *Bernoulli* **23**(4A), 2917–2950 (2017)
- Voliotis, M., Thomas, P., Grima, R., Bowsher, C.G.: Stochastic simulation of biomolecular networks in dynamic environments. *PLoS computational biology* **12**(6), 1004923 (2016)
- Wqvist, S., Frellsen, J., Picchini, U.: Sequential neural posterior and likelihood approximation. *arXiv preprint arXiv:2102.06522* (2021)
- Whitaker, G.A., Golightly, A., Boys, R.J., Sherlock, C.: Bayesian inference for diffusion-driven mixed-effects models. *Bayesian Analysis* **2**(12), 435–463 (2017)
- Wqvist, S., Golightly, A., McLean, A.T., Picchini, U.: Efficient inference for stochastic differential equation mixed-effects models using correlated particle pseudo-marginal algorithms. *Computational Statistics & Data Analysis* **157**, 107151 (2021)
- Wang, X., Kelly, R.P., Jenner, A.L., Warne, D.J., Drovandi, C.: A comprehensive guide to simulation-based inference in computational biology. *arXiv preprint arXiv:2409.19675* (2024)
- Wqvist, S., Mattei, P.-A., Picchini, U., Frellsen, J.: Partially exchangeable networks and architectures for learning summary statistics in approximate Bayesian computation. In: *Proceedings of the 36th International Conference on Machine Learning*, vol. 97, pp. 6798–6807 (2019)
- Wood, S.N.: Statistical inference for noisy non-linear ecological dynamic systems. *Nature* **466**(7310), 1102–1104 (2010)
- Xu, L., Jordan, M., Hinton, G.E.: An alternative model for mixtures of experts. *Advances in neural information processing systems* **7** (1994)



## Appendix A Conjugate priors for the Ornstein-Uhlenbeck model

For the Ornstein-Uhlenbeck model we use conjugate priors, as a matter of convenience, as it makes it easier to compare the results of SeM-PLP with the gold standard inference obtained using the Kalman filter. With conjugate priors we can sample explicitly from equation (25), and this is achieved by setting a Normal-Gamma prior distribution on the population parameters  $\boldsymbol{\eta}$  as following

$$\begin{cases} \mu_j | \tau_j \sim \mathcal{N}(\mu_{0j}, (\lambda_j \tau_j)^{-1}), & j = 1, 2, 3 \\ \tau_j \sim \text{Ga}(\alpha_j, \beta_j). \end{cases} \quad (\text{A1})$$

We denote the latter prior by Normal-Gamma( $\boldsymbol{\mu}, \boldsymbol{\lambda}, \boldsymbol{\alpha}, \boldsymbol{\beta}$ ), and we let the population distribution be a Gaussian  $\pi(\mathbf{c} | \boldsymbol{\eta}) \sim \mathcal{N}(\boldsymbol{\mu}, \boldsymbol{\tau}^{-1})$ . The distribution that we want to sample from in (25) is therefore a Normal-Gamma distribution (Murphy 2007) with the following parameters

$$\text{NG}\left(\frac{\lambda_j \mu_{0j} + M \bar{c}_j}{\lambda_j + M}, \lambda_j + M, \alpha_j + M/2, \beta_j + \frac{1}{2} \sum_{i=1}^M (c_j^{(i)} - \bar{c}_j)^2 + \frac{M \lambda_j}{\lambda_j + M} \frac{(\bar{c}_j - \mu_{0j})^2}{2}\right).$$

## Appendix B Determination of $K$

The number  $K$  of components in the Gaussian mixture model has to be specified prior to performing the EM procedure. A too large value of  $K$  may result in overfitting and unnecessary computational effort, while a too small value of  $K$  may limit the ability to represent the relationship between  $\boldsymbol{\theta}$  and  $\mathbf{y}$ . The Bayesian Information Criterion (BIC), used in Deleforge et al. (2014) and

Häggström et al. (2024) to guide the selection of  $K$ , is given by

$$\text{BIC} = -2\mathcal{L}(\hat{\boldsymbol{\phi}}) + D(\tilde{\boldsymbol{\phi}}) \log N$$

where  $\mathcal{L}(\hat{\boldsymbol{\phi}})$  is the maximised value of the GLLiM log-likelihood function at the MLE  $\hat{\boldsymbol{\phi}}$ ,  $D(\tilde{\boldsymbol{\phi}})$  is the total number of parameters in the model and  $N$  is the number of observations in the training dataset. We wish to select a  $K$  returning a small BIC when GLLiM is fitted with  $K$  components to a training dataset  $\{\boldsymbol{\theta}_n, \mathbf{y}_n\}_{n=1}^N$  obtained by independently sampling parameters  $\boldsymbol{\theta}_n \sim p(\boldsymbol{\theta})$  from the prior and simulating the corresponding  $\mathbf{y}_n \sim p(\mathbf{y} | \boldsymbol{\theta}_n)$  from the generative model. When the “data” is the set of the  $N$  independent  $\{\boldsymbol{\theta}_n, \mathbf{y}_n\}_{n=1}^N$ , the GLLiM log-likelihood is given by

$$\mathcal{L}(\tilde{\boldsymbol{\phi}}) = \sum_{n=1}^N \log q_{\tilde{\boldsymbol{\phi}}}(\mathbf{y}_n, \boldsymbol{\theta}_n),$$

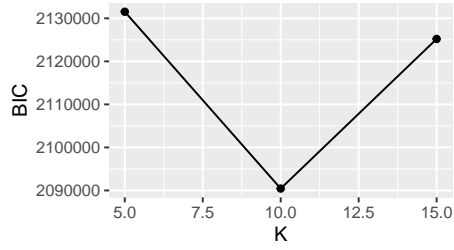
with

$$q_{\tilde{\boldsymbol{\phi}}}(\mathbf{y}_n, \boldsymbol{\theta}_n) = \prod_{k=1}^K \mathcal{N}(\mathbf{y}_n; \tilde{\mathbf{A}}_k \boldsymbol{\theta}_n + \tilde{\mathbf{b}}_k, \tilde{\boldsymbol{\Sigma}}_k) \mathcal{N}(\boldsymbol{\theta}_n; \tilde{\mathbf{c}}_k, \tilde{\boldsymbol{\Gamma}}_k) \pi_k.$$

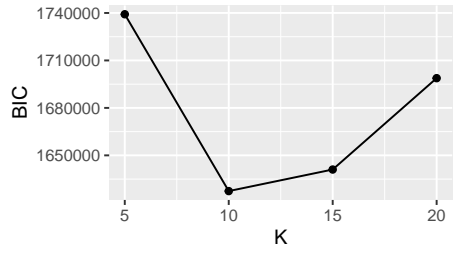
Note that within our framework  $\boldsymbol{\theta} = (\mathbf{c}, \boldsymbol{\kappa}, \boldsymbol{\xi})$  and thus  $l = q + p + s$ , where  $\boldsymbol{\theta} \in \mathbb{R}^l$ , and  $\mathbf{y} \in \mathbb{R}^{d_o n}$ , where  $d_o$  is the dimension of the observation at a specific time point and  $n$  is the number of time points in the observation. The number of parameters that GLLiM needs to estimate is

$$D(\tilde{\boldsymbol{\phi}}) = (K - 1) + K(d_o n(q + p + s) + d_o n + (q + p + s) + \text{nbpar}_{\boldsymbol{\Sigma}} + \text{nbpar}_{\boldsymbol{\Gamma}}), \quad (\text{B2})$$

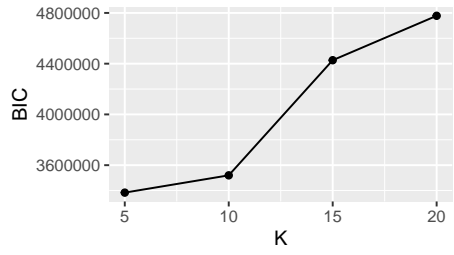
where  $\text{nbpar}_{\boldsymbol{\Sigma}}$  and  $\text{nbpar}_{\boldsymbol{\Gamma}}$  are the number of parameters in the covariance matrices  $\tilde{\boldsymbol{\Sigma}}_k$  and  $\tilde{\boldsymbol{\Gamma}}_k$ , respectively. The covariance structure of the matrices  $\tilde{\boldsymbol{\Sigma}}_k$  and  $\tilde{\boldsymbol{\Gamma}}_k$  can be constrained to reduce the number of parameters that GLLiM needs to estimate. The xLLiM package (Perthame et al. 2022), that we use to run Expectation-Maximization when fitting GLLiM models, allows the  $\tilde{\boldsymbol{\Sigma}}_k$ ’s to be set as isotropic, diagonal or full matrices, and set all equal or varying with  $k$ . The setup we considered for the covariance matrices can be found in the sections pertaining each of the considered examples.



(a)



(b)



(c)

**Fig. B1:** Bayesian information criterion as a function of  $K$ . (a) Ornstein-Uhlenbeck model. (b) mRNA model with simulated data. (c) mRNA model with real data (40 subjects).

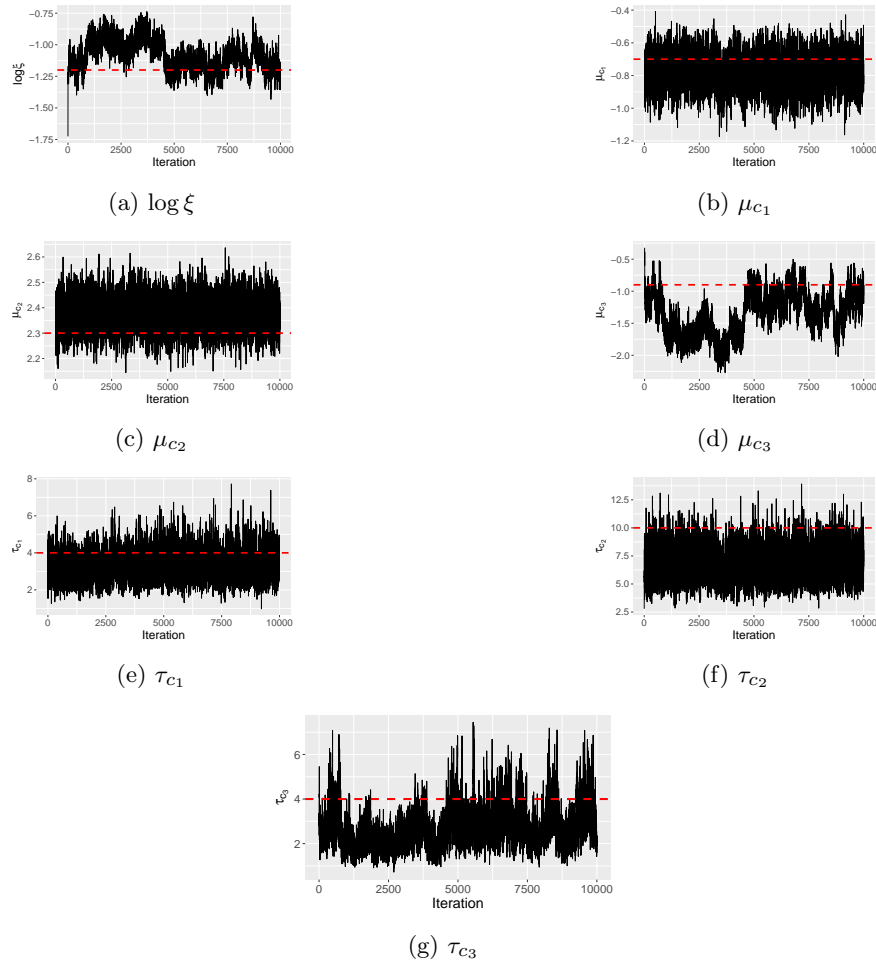
## S3 Supplementary Material

### S3.1 Ornstein-Uhlenbeck

The prior parameters were set to

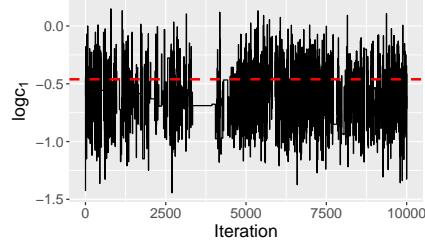
$$\begin{aligned}(\mu_{0_1}, \lambda_1, \alpha_1, \beta_1) &= (0, 1, 6, 2), \\(\mu_{0_2}, \lambda_2, \alpha_2, \beta_2) &= (1.5, 1, 6, 1), \\(\mu_{0_3}, \lambda_3, \alpha_3, \beta_3) &= (0, 1, 6, 2).\end{aligned}$$

Figure S1 shows the traceplots obtained from round 2 of SeMPLE for the “common” (shared between subjects) parameters  $\boldsymbol{\eta} = (\mu_1, \mu_2, \mu_3, \tau_1, \tau_2, \tau_3)$  and  $\boldsymbol{\xi}$ . Notice that for iterations when  $\mu_{c_3}$  is overestimated,  $\log \xi$  is underestimated, and the other way around.

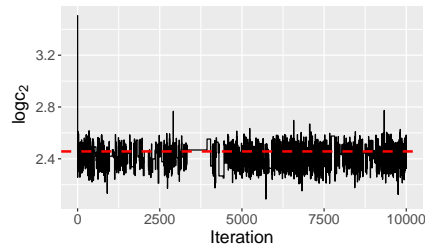


**Fig. S1:** Ornstein-Uhlenbeck, traceplots of posterior samples from round 2 of SeMPLE for the “common” parameters  $\boldsymbol{\eta} = (\mu_1, \mu_2, \mu_3, \tau_1, \tau_2, \tau_3)$  and  $\boldsymbol{\xi}$ . The red dashed line shows the true value used to generate the observed data.

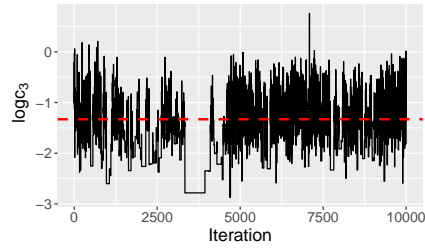
Inference for individual parameters  $\log \mathbf{c}^{(i)} = (\log c_1^{(i)}, \log c_2^{(i)}, \log c_3^{(i)})$  is in Figure S3. We considered  $M = 40$  subjects and therefore, given the large numbers of possible plots to display, as an illustration, we report inference for the first five subjects only,  $i = 1, \dots, 5$ . The inference from SeMPLE is remarkably accurate, as the posteriors capture the true values of the  $\log \mathbf{c}^{(i)}$ 's while clearly producing a noticeable learning compared to the corresponding priors.



(a)  $\log c_1^{(1)}$



(b)  $\log c_2^{(1)}$



(c)  $\log c_3^{(1)}$

**Fig. S2:** Ornstein-Uhlenbeck, traceplots of inference from SeMPLE for individual parameters for individual 1 out of 40: traceplots are from round 2 of SeMPLE. The red dashed line shows the true value of this specific individual.

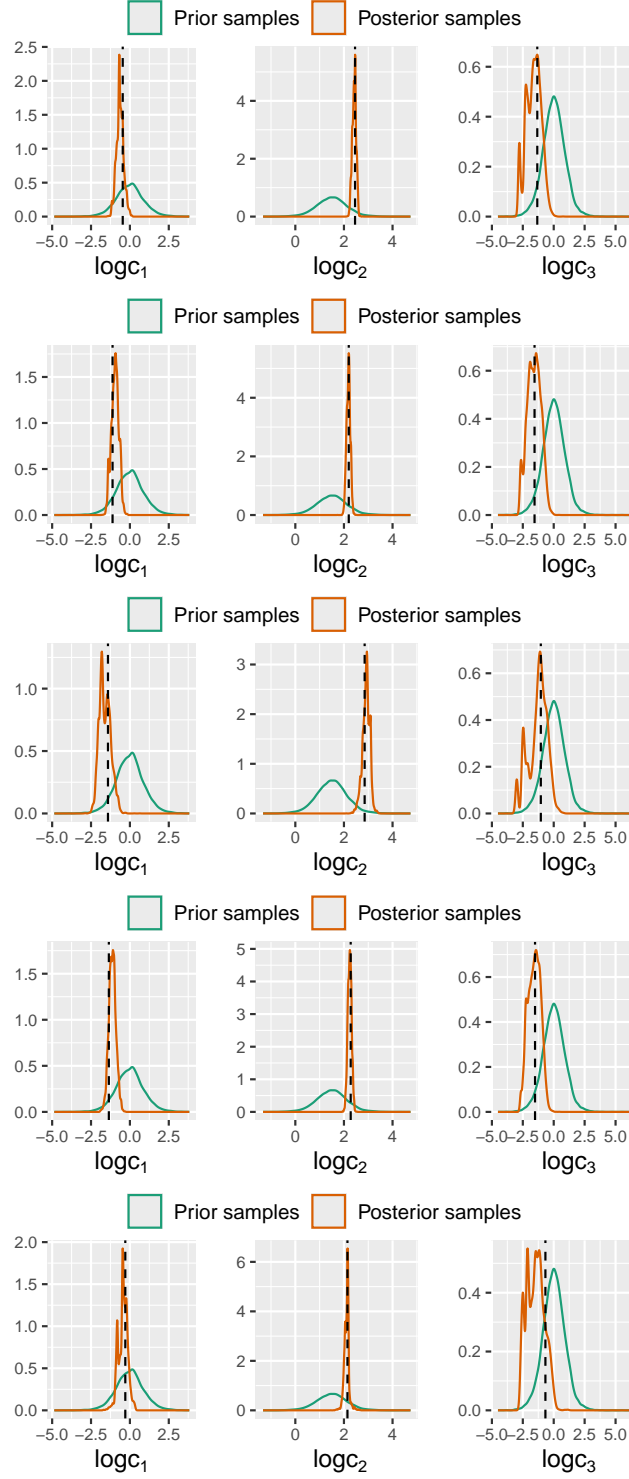


**Fig. S3:** Ornstein-Uhlenbeck, inference from SeMPLE: in orange are the kernel density estimates of posterior samples from round 2 of SeMPLE for the individual parameters  $\log c^{(i)}$ . Individual 1 to 5 out of 40. The prior is in green. The red dashed lines show the true parameters for this specific individual.



### S3.2 mRNA model: simulated data

The prior distributions are set to be Normal-Gamma for the random effects

$$\begin{cases} \mu_j | \tau_j \sim \mathcal{N}(\mu_{0j}, (\lambda_j \tau_j)^{-1}) \\ \tau_j \sim Ga(\alpha_j, \beta_j), \quad j = \delta, \gamma, k, \end{cases} \quad (C3)$$

where

$$\begin{aligned} (\mu_{0\delta}, \lambda_\delta, \alpha_\delta, \beta_\delta) &= (-0.694, 1, 2, 0.5), \\ (\mu_{0\gamma}, \lambda_\gamma, \alpha_\gamma, \beta_\gamma) &= (-3, 1, 2, 0.5), \\ (\mu_{0k}, \lambda_k, \alpha_k, \beta_k) &= (0.027, 1, 2, 0.5), \end{aligned}$$

and the fixed effects have Gaussian priors on the log-scale  $\log m_0 \sim \mathcal{N}(5, 1)$ ,  $\log \text{scale} \sim \mathcal{N}(1, 1)$ ,  $\log \text{offset} \sim \mathcal{N}(3, 1)$ ,  $\log \xi \sim \mathcal{N}(-1.5, 1)$ .

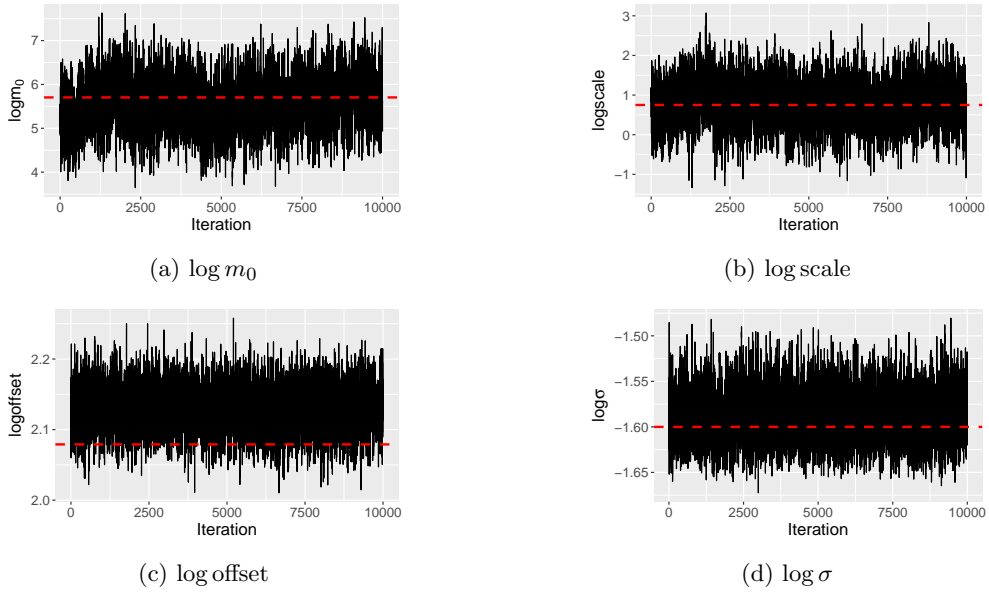
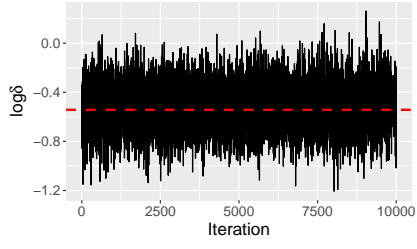
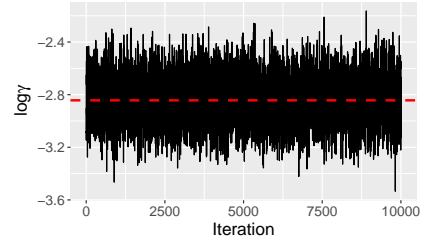


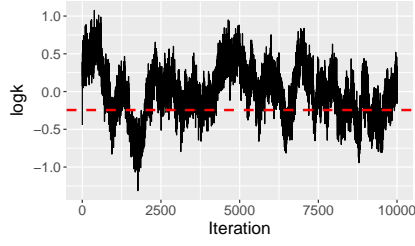
**Fig. S4:** mRNA model with simulated data: SeMPLE traceplots of population parameters from SeMPLE round 2. The red dashed line shows the true parameter values.



(a)  $\log \delta^{(1)}$



(b)  $\log \gamma^{(1)}$



(c)  $\log \kappa^{(1)}$

**Fig. S5:** mRNA model with simulated data, traceplots for individual parameters from round 2 of SeMPLE for individual 1 out of 40. The red dashed lines show the true parameters for this specific individual.

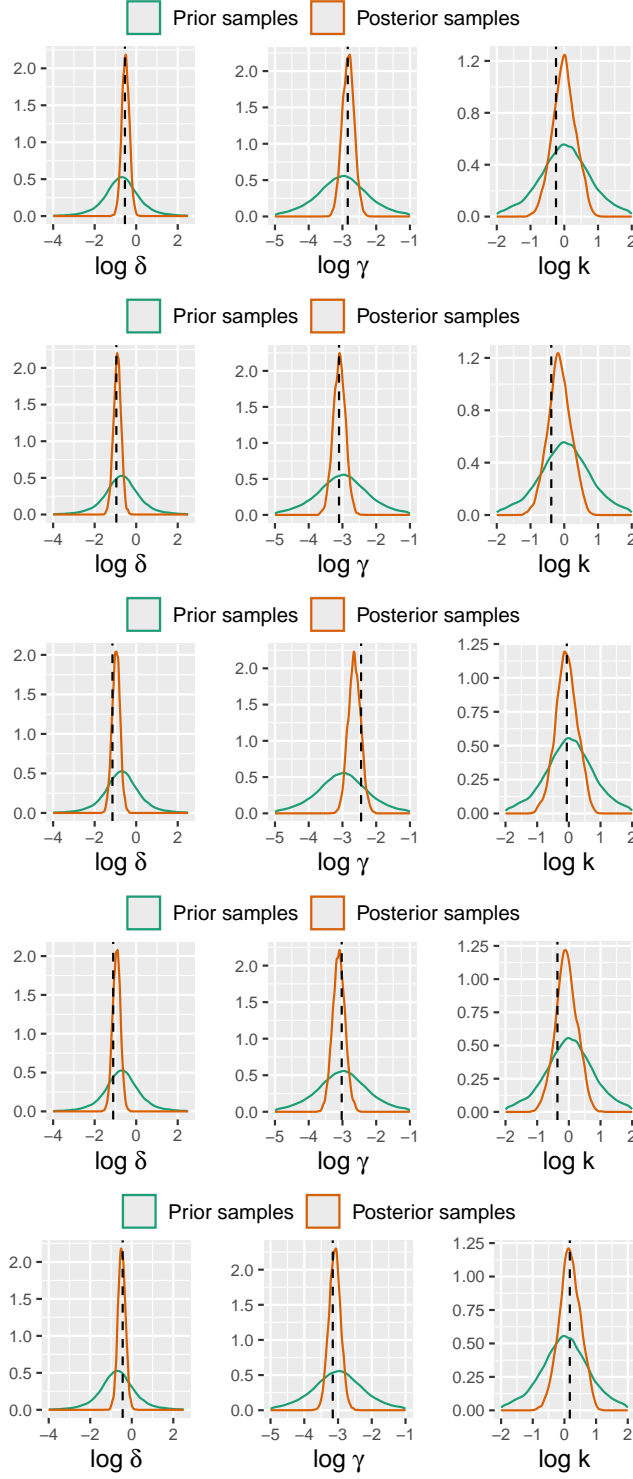


**Fig. S6:** mRNA with simulated data: marginal posteriors from round 2 of SeMPLE for the individual parameters ( $\log \delta^{(i)}$ ,  $\log \gamma^{(i)}$ ,  $\log \kappa^{(i)}$ ) of the first 5 individuals out of 40. The black dashed lines shows the true parameter values of each specific individual.

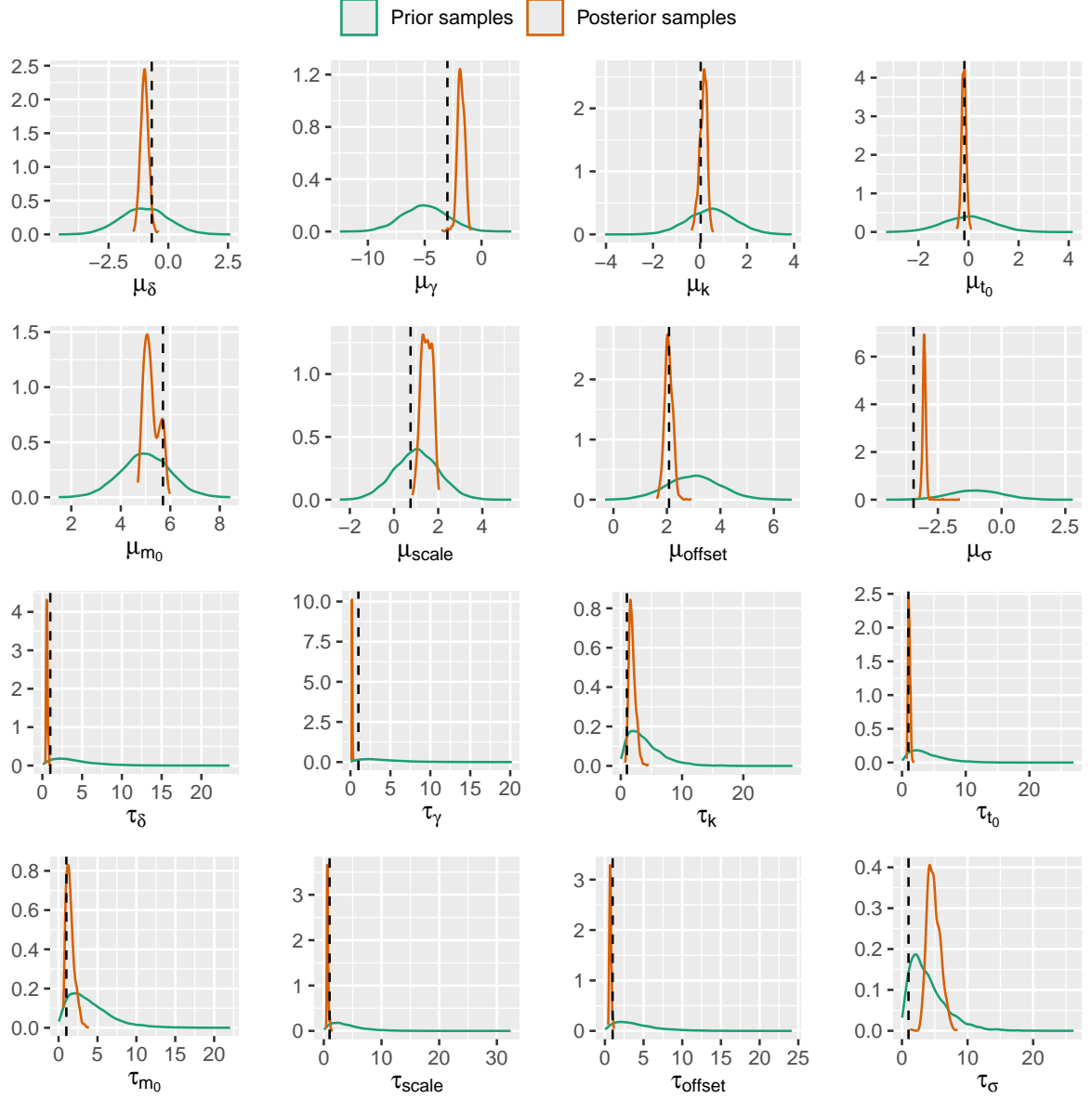


**Fig. S7:** mRNA model with simulated data from 200 individuals when assuming that all parameters are random effects: marginal posteriors obtained with SeMPLE (orange) and priors (green). Note that the true population precision  $\tau = 1$  for all parameters. The marginal posteriors are based on 10k posterior samples.

## S4 mRNA model: real data

In the inference setup with real data the priors are set to

$$\begin{cases} \mu_j \sim \mathcal{N}(\mu_{0j}, \sigma_j^2) \\ \tau_j \sim \text{Ga}(\alpha_j, \beta_j), \end{cases} \quad j = \delta, \gamma, k, t_0. \quad (\text{D4})$$

where

$$\begin{aligned}(\mu_{0\delta}, \sigma_\delta, \alpha_\delta, \beta_\delta) &= (-1, 1, 2, 0.5), \\(\mu_{0\gamma}, \sigma_\gamma, \alpha_\gamma, \beta_\gamma) &= (-5, 2, 2, 0.5), \\(\mu_{0k}, \sigma_k, \alpha_k, \beta_k) &= (0.5, 1, 2, 0.5), \\(\mu_{0t_0}, \sigma_{t_0}, \alpha_{t_0}, \beta_{t_0}) &= (0, 1, 2, 0.5),\end{aligned}$$

and  $\log m_0 \sim \mathcal{N}(5, 1)$ ,  $\log \text{scale} \sim \mathcal{N}(1, 1)$ ,  $\log \text{offset} \sim \mathcal{N}(3, 1)$ ,  $\log \sigma \sim \mathcal{N}(-1, 1)$ .

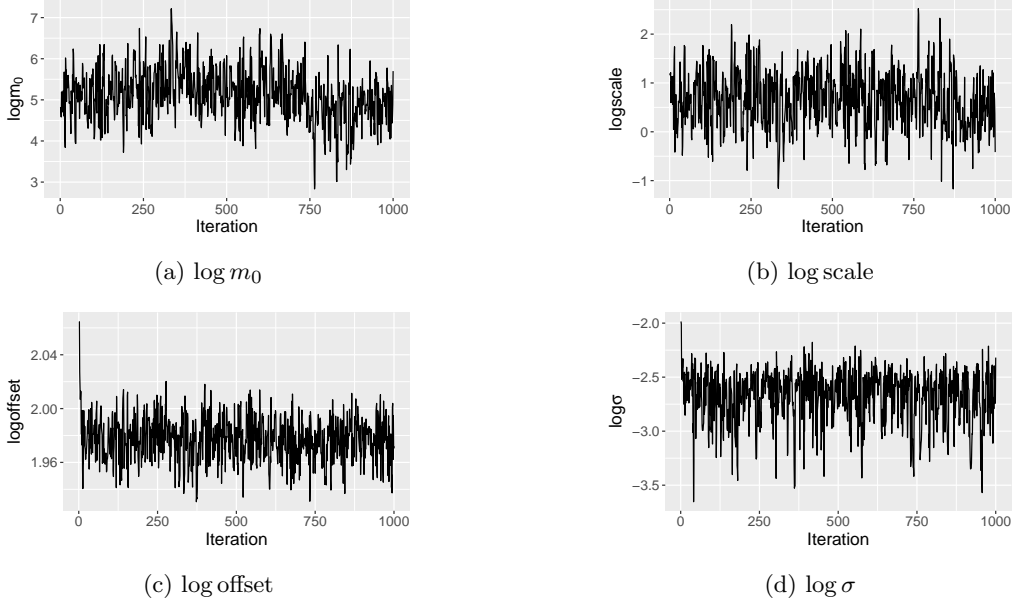
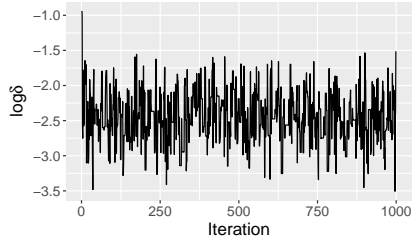
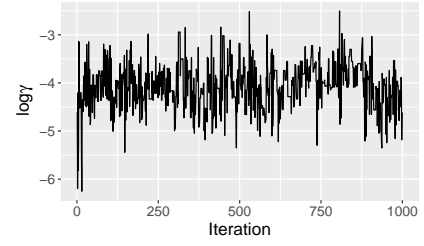


**Fig. S8:** mRNA model with real data: traceplots of constant parameters from round 2 of SeMPLE.

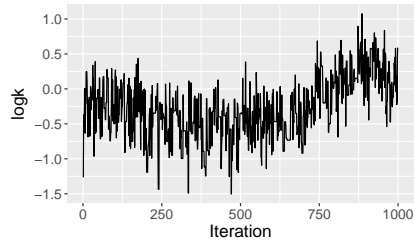




(a)  $\log \delta$



(b)  $\log \gamma$



(c)  $\log \kappa$

**Fig. S9:** mRNA model with real data, inference from SeMPLE for individual 1 out of 40: traceplots from round 2 of SeMPLE.

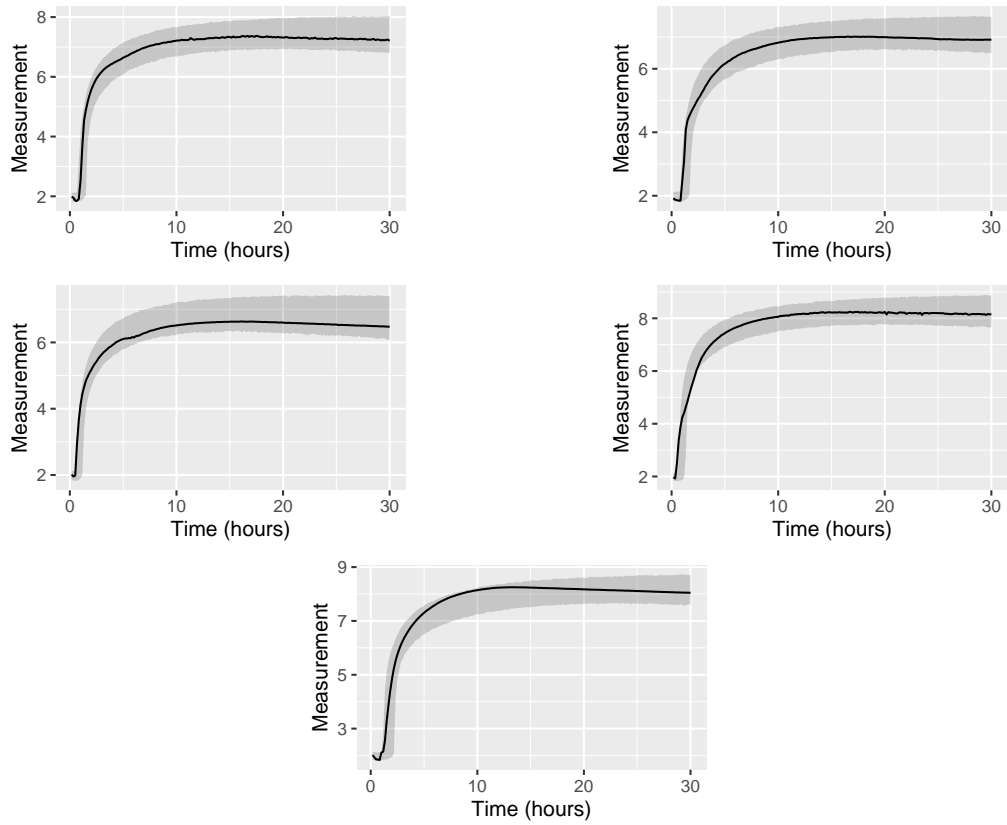


**Fig. S10:** mRNA model with real data: Posterior-predictive simulations based on 10k individual specific SeMPLE posterior samples for the first 5 individuals (top left to bottom right). The black line shows the observed trajectory of each individual. In gray is the area between the 2.5th and 97.5th percentile.

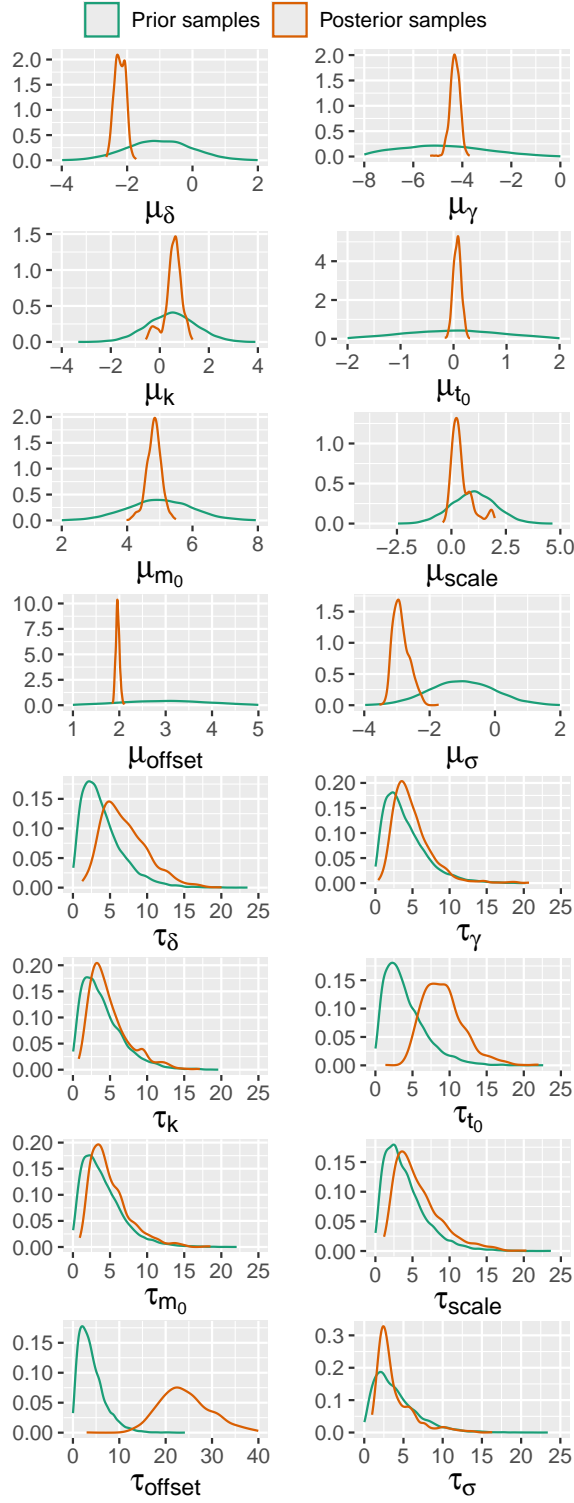


**Fig. S11:** mRNA model with real data when assuming that all parameters are random effects: marginal posteriors obtained with SeMPLE (orange) and priors (green).